Effect of Chromium and Manganese on Corrosion Behavior of Fe-TiC Composites

Izumi N. Reed
B.S., Oregon Institute of Technology, U.S.A., 1996

A thesis presented to the faculty of the
Oregon Graduate Institute of Science and Technology
in partial fulfillment of the
requirements for the degree
Master of Science
in
Materials Science and Engineering

October 1998

This thesis "Effect of Chromium and Manganese on Corrosion Behavior of Fe-TiC Composites" by Izumi N. Reed has been examined and approved by the following Examination Committee:

Margaret Ziomek-Moroz, Thesis Advisor
Associate Professor

Dr. Jeffrey A. Hawk
U.S. Department of Energy
Albany Research Center

Dr. Ömer Doğan
U.S. Department of Energy
Albany Research Center

Lemmy Meekisho
Associate Professor

Dedication

Dedication to my parents, Mokoto and Nobuko

And my husband, Joel.

Acknowledgements

I would like to thank my thesis advisor, Dr. Margaret Ziomek-Moroz for her guidance. I am grateful to Dr. Jeffrey Hawk and Dr. Ömer Doğan from the U. S. Department of Energy, Albany Research Center for their very helpful suggestions. I would also like to thank my other committee member, Dr. Lemmy Meekisho for reviewing the manuscript. The financial support of this research by TAPPI Foundation is gratefully acknowledged. I would like to thank for the support and help by Jim Van Winkle, David Turcio, Robert Davis, and Jinhong Yang of the Department of Materials Science and Engineering at Oregon Graduate Institute of Science and Technology. I would also like to thank Dr. Wei Su of Engineering Animation for his help and support.

I would like to thank my father, Mokoto who inspired and motivated me to become an engineer. I also would like to thank my mother, Nobuko and my husband, Joel for their support.

Table of Contents

List of Tables

List of Figures

Abstract

Effect of Chromium and Manganese on Corrosion Behavior of Fe-TiC Composites

Izumi N. Reed

Supervising Professor: Dr. Margaret Ziomek-Moroz

The goal of this thesis is to determine the corrosion behavior of a new class of advanced materials, namely: titanium carbide reinforced iron composites containing chromium (Fe-Cr-TiC) and chromium and manganese (Fe-Cr-Mn-TiC). TiC has excellent physical properties, such as high melting point, low density, high Vickers hardness value, high electrical resistivity and low thermal expansion. Due to their great wear resistance characteristics and toughness, these materials show potential applications in pulp and paper industries, mining and mineral processing industries, metallurgical industries, cement industries, and electric industries. Some components made of these materials may work under a combined action of corrosion and wear. This study is aimed at determining the corrosion behavior using electrochemical methods such as potentiodynamic and potentiostatic. Two different electrolytes were used in this research: 1N (0.5 M) sulfuric acid (H_2SO_4) and 1N (0.5 M) sodium sulfate (Na_2SO_4). The experiments were performed on the following materials; Fe-TiC, Fe-Cr-TiC, Fe-Cr-Mn-TiC and their matrix materials.

Chapter 1
Introduction

1.1 What Are Metal Matrix Composites?

Generally, the man made materials that contain two different chemicals or materials and a specific interface separating the elements are called composites.[1] Composites are generally fabricated to achieve better properties that cannot be obtained by each constituent element. Metal matrix composites (MMC) consist of at least one metal matrix and one or more reinforcements. In most cases, MMC can achieve higher toughness, strength, stiffness and impact properties, and better electrical and thermal properties than their constituent elements or alloys. [2] The processing of MMC is different from the processing of multi-phase alloys. When MMC are fabricated, a matrix and reinforcement are mixed together. MMC usually have very superior mechanical properties in extreme conditions and environment. A metallic phase material that can be a matrix is mixed with an another phase (reinforcement). One of MMC is Al-SiC that is a mixture of aluminum (matrix) and silicon carbide (reinforcement).[1] Another example of MMC is Fe-TiC that is a mixture of iron (Fe) and titanium carbide (reinforcement).

Some MMC stress-strain curves show three stages. The first stage represents elastic deformation of both the matrix and the fiber or the reinforcements. The second stage usually represents the matrix deforming from elastic to plastic while the fiber or the reinforcements still remain elastic. The last stage represents both the matrix and the fiber or the reinforcements that undergo plastic deformation. Other MMC stress-strain

curves only show two stages that usually are stage one and stage three.

Thermal stress may be caused by the different temperature gradients within the composites, or the different thermal expansion of matrix and reinforcement under constant temperature. So, it is important to know the properties of each constituent element when designing MMC. [1]

1.2 What Is TiC?

In TiC, the covalent bonding between titanium and carbon is very strong. The melting point of TiC is 3067 °C that is much higher than that of titanium. Its molecular weight is 59.91 g/mol. The color is silver gray. It is a good electrical conductor. The thermal conductivity is 21 W/m °C. The thermal expansion is $7.4x10^{-6}$/°C. Vickers hardness is 28 ~ 35 GPa. Oxidation starts slowly in the air around 800 °C. The metal to carbon ratio affects magnetic susceptibility. TiC is very resistant to most chemicals and acids except HNO_3 and HF. Therefore, this material is suited for high temperature environment applications.[3]

1.3 Fabrication Methods of Fe-TiC

In most cases, MMCs are fabricated using reinforcement such as long fibers, short fibers, short whiskers or small particles (e.g. tungsten, silicon carbides and carbon). Then, they are added into matrix (e.g. aluminum) to form MMCs. The fabrication processing technologies of Fe-TiC at the U.S. Department of Energy, Albany Research Center involves powder metallurgy and melt-solidification processing.[4]

The powder metallurgical processes of Fe-TiC can be achieved by sintering TiC powders with Fe based matrix powders or self-propagating high-temperature synthesis (SHS) processing of elemental powders of Fe, Ti and C. These technologies are described in Chapter 1.3.1.

The melt-solidification processes of Fe-TiC composites involve addition of TiC powders in an iron-based melt or *in-situ* reaction described in Chapter 1.3.2.[4]

1.3.1 Powder Metallurgical Technology

To obtain Fe-TiC composites by sintering, TiC powder is added to Fe based matrix powder.[4] Then, processed by pressing the powder to a desired shape followed by the liquid phases sintering, the reaction sintering, or the hot pressing (pressure sintering). Some of the powder pressing techniques are tape casting, extrusion, injection molding, isostatic pressing, and slip casting. Sintering is a process to bond powder particles together. It causes shrinkage, densification, and grain growth. To achieve good final products, powder particles should be small, have equiaxed shape and high purity. There are a few criteria that must be fulfilled to complete sintering. For liquid sintering, it is important to have liquid or molten metal that can wet the solid at sintering temperature. It is also important that solids have good solubility properties in liquid or molten metal. For reaction sintering, it is necessary to add additives to start the reaction. Pressure sintering requires high pressured gas, high temperature and/or vacuums environments. [3]

The other process is called Self-propagating High-temperature Synthesis (SHS). SHS is one of the processes for joining similar or dissimilar advanced materials and hybrid structures using exothermic reaction. Moreover, this process is another manufacturing method for powders used in powder metallurgy and ceramic materials. It can decrease the processing time and energy input, and produces relatively pure composites. [5, 6]

The SHS process is a result of reactions between metals and non-metals or gases using exothermic reaction. The SHS uses constituent elements of powders. For instance, precipitate of TiC is formed by the SHS reaction of titanium and carbon powders.[4] Another example is tungsten reacts with carbon to produce tungsten carbide. SHS processing usually starts by mixing and compressing powders into desired shapes before synthesizing. After the desired shape is achieved, an energy source is added to initiate the process. The energy source can be a heated filament, laser or etc. Usually, this energy source, which is added to the one end of compacted materials, becomes a combustion

wave that is carrying energy though the entire composites without additional external energy. [3, 6]

1.3.2 Melt-Solidification Processing Technology

During the melt solidification process of Fe-TiC composites, there could be a few problems that may result in segregation of constituent phase creating an uneven distribution of carbide particles in the composites caused by the different densities between the ferrous matrix and the TiC precipitate phase. However, it is possible to produce small samples without such problems by using an electromagnetic stirring technique and a levitation technique. [4]

Another melt solidification processing technology is called *in-situ* process. This process starts with a liquid metal (matrix). Then, the liquid metal reacts with the injected gas to form a ceramic reinforcement. For instance, TiC reinforced aluminum copper alloys are produced by CH_4 and argon gas injected into Al-Cu-Ti melt. Another *in situ* process involves directional solidification of the liquid metal to form composite. For this technique, the titanium is added to a liquid high-carbon iron mixture.[4] By exothermic reaction, the TiC precipitates are formed as a result.[4] After that, composite ingots or cast parts are produced. [2]

1.4 Corrosion and Wear Behavior of Fe and TiC

Fe-TiC composites show great promise for corrosive wear applications because of their excellent abrasion resistance. There is no literature available for Fe-TiC composite concerning their corrosion behavior in aqueous solutions and the role of corrosion in corrosive wear. There is some literature data available for the matrix (Fe) and reinforcement (TiC) on corrosion and wear behavior.

For example, high carbon steel contains 0.7 percent – 1.0 percent carbon is used in many applications because of their good wear resistance and hardness. [7] It passivates in alkaline solutions with high pH at ambient temperature. However, it pits in neutral and alkaline salt solutions containing chloride.[7] It might corrode without proper coating or other protection; therefore, it is not suited for corrosive wear application.

TiC is sometimes used for coatings on steel to improve corrosion resistance. It has been documented that TiC coatings on the steel decreased corrosion rate, dissolution and passive current density when they are compared with bare steel.[8]

Furthermore, chromium and manganese are added to Fe-TiC composites. The addition of chromium to the iron would improve impact strength, oxidation and corrosion resistance.[9] Also, manganese and chromium are classified as carbide stabilizers.[10] Iron based alloys having at least 12 percent chromium passivate in most dilute aerated solutions. [7]

The abrasive wear tests performed on Fe-TiC and Fe-TiC-Cr composites show that the high purity iron exhibits higher wear rate than the carbide reinforced composites. Moreover, the addition of chromium to Fe-TiC composites improved their wear rate. Furthermore, Fe-Cr-TiC composite showed much better abrasive wear rate than white cast iron.[4]

Chapter 2
Research Objectives

The main goal of this research was to determine the corrosion behavior of Fe-TiC reinforced composites in 1N sulfuric acid and 1N sodium sulfate. Fe-TiC reinforced composites were compared with Fe-Cr-TiC and Fe-Cr-Mn-TiC to determine the effect of addition of chromium and manganese on the corrosion behavior in these environments. Additionally, the corrosion behavior of Fe-TiC reinforced composites were compared to their pure matrix composites to determine the effect of TiC. In order to accomplish the goal, potentiodynamic and potentiostatic experiments were carried out. Also, their open circuit potential values were determined in H_2SO_4 and Na_2SO_4.

Chapter 3
Experimental Procedures

Due to the electrochemical nature of the corrosion process occurring in this system, the electrochemical techniques were used to determine their corrosion characteristics. Potentiodynamic experiments were used to compare the corrosion resistance of the samples that were used during this research in a specific environment.

The setup used for the potentiodynamic, potentiostatic, and open circuit, also called free corrosion potential (Ecorr) experiments is shown in Figure 3-1. EG & G Princeton Applied Research Potentiostat / Galvanostat Model 273A was connected to an IBM compatible PC to collect data. All the data were plotted by using KaleidaGraph.

3.1 Electrolytes

The experiments were performed in 1 N (0.5 M) sulfuric acid (H_2SO_4) and 1 N (0.5 M) sodium sulfate (Na_2SO_4) because some of the electrolytes present in the pulp and paper industry contain sulfur. Moreover, the literature data and Pourbaix diagram conformed that Fe dissolves at low pH and passivates at neutral pH. The experiments were curried out in non-deaerated solutions at room temperature.

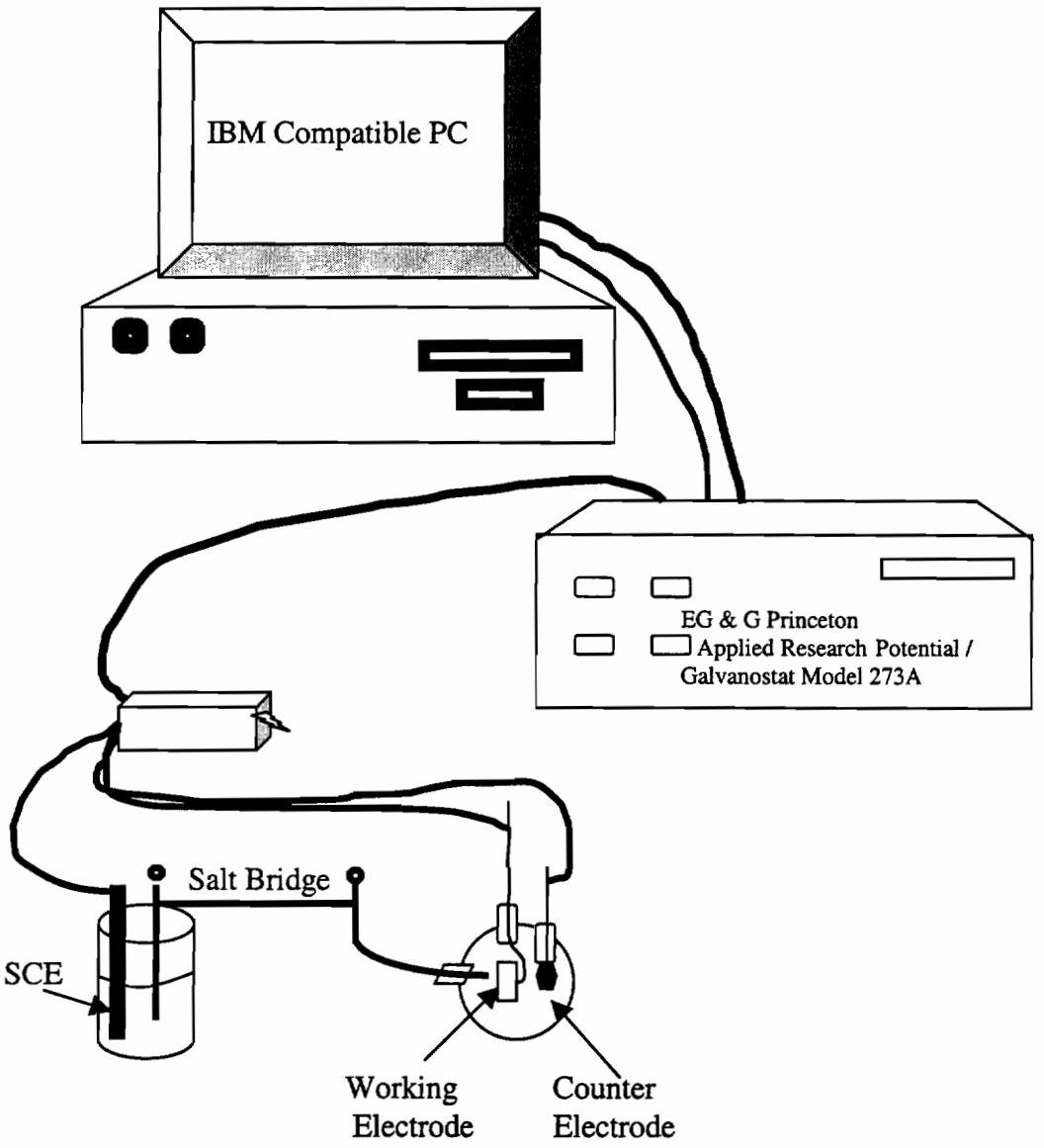

Figure 3-1. Experimental Setup

3.2 Specimens

The chemical composition of the materials used during this research is listed in Table 3-2-1 (composites) and Table 3-2-2 (matrix of composites). All materials were prepared at the U. S. Department of Energy, Albany Research Center. The composites were manufactured by melting a charge of electrolytic Fe, C, Mn, and sorel iron in a vacuum induction furnace. When the vacuum chamber of the induction furnace reached the maximum vacuum level, it was filled with argon gas until 1/3 of atmospheric pressure was reached. Before the chamber was closed, ferrotitanium was placed in a scoop that could be handled from outside. After the charge was melted, the molten alloy was heated for additional 5 minutes. During these 5 minutes, the ferrotitanium was added gradually into the molten alloy, and stirred by intuitive forces. Before the molten alloy was poured into a graphite mold, it was held inside the furnace for another 3 minutes. To minimize the shrinkage, a hot tub was used.

Table 3-2-1. Chemical Composition of Fe-TiC, Fe-Cr-TiC, and Fe-Cr-Mn-TiC

Material	Compositions (numbers are wt. %)	
Fe-Cr-Mn-TiC	4.21 **Ti**, 1.81 **C**, 14.9 **Cr**, 13.5 **Mn**	1.13 **Si**, 0.13 **O**
Fe-TiC	1.27 **Ti**, 1.61 **C**	0.095 **Si**, 0.0553 **O**
Fe-Cr-TiC	1.34 **Ti**, 1.74 **C**, 19.2 **Cr**	0.111 **Si**, 0.0707 **O**

Table 3-2-2. Chemical Composition of matrix of Fe-TiC, Fe-Cr-TiC, and Fe-Cr-Mn-TiC

Material	Compositions	(numbers are wt. %)
Matrix of Fe-Cr-Mn-TiC	0.8 **C**, 14.9 **Cr**, 13.5 **Mn**	1.10 **Si**
Matrix of Fe-TiC	1.30 **C**	0.10 **Si**
Matrix of Fe-Cr-TiC	1.42 **C**, 19.2 **Cr**	0.10 **Si**

Figure 3-2-1 shows specimen geometry. The back face of each specimen was spot welded with a copper wire to achieve electrical contact. A Teflon tube protected the copper wire from corrosion. The specimens were flat round pieces approximately 1.5 cm in diameter. The specimens were mounted in epoxy. A 600-grit silicon carbide paper was used to polish the specimen surface before each experiment.

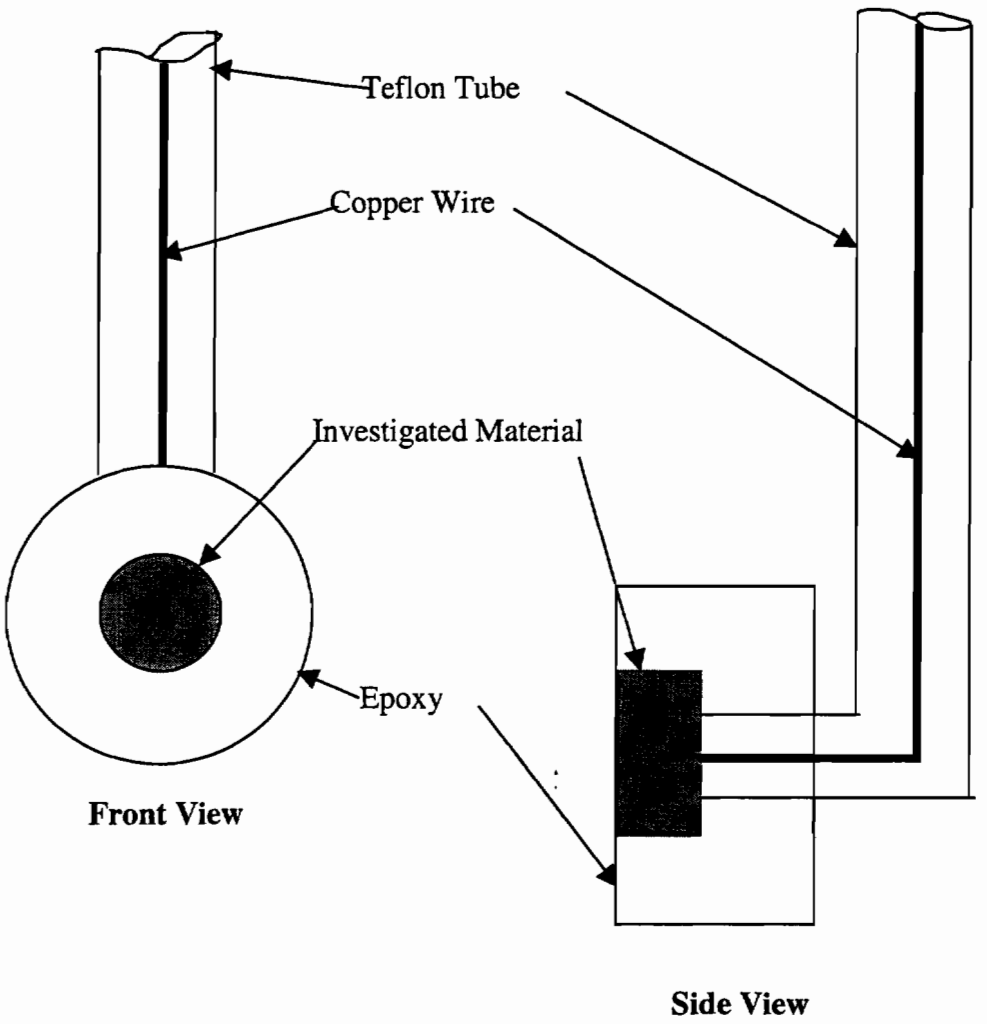

Figure 3-2-1. Specimen Geometry

3.3 Microscopic Observation

Figure 3-3-1 shows an optical micrograph of Fe-Cr-Mn-TiC (500X). TiC is distributed evenly. As an example, as it shown, TiC particles are distributed uniformly.

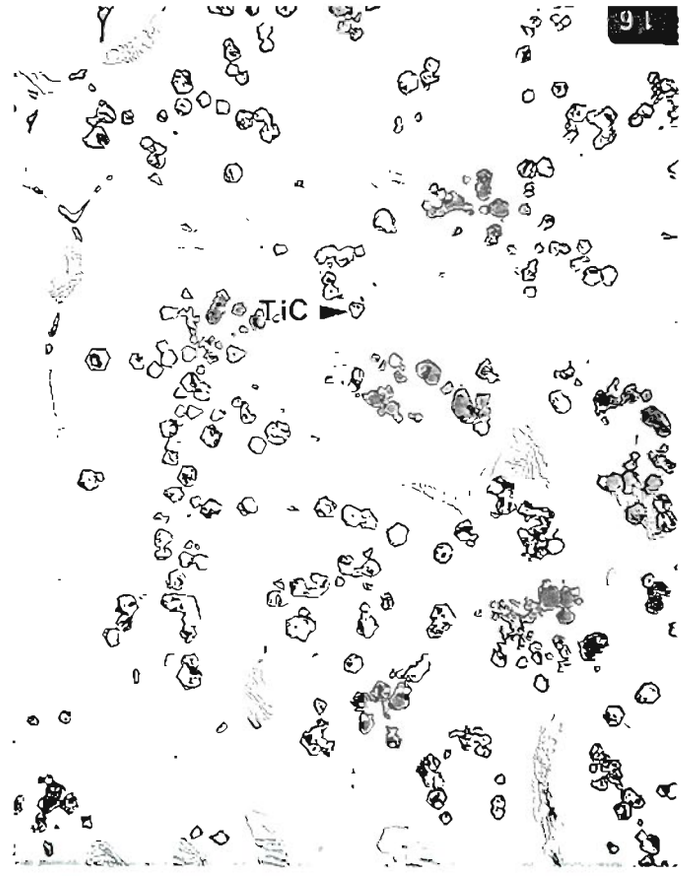

Figure 3-3-1. Optical Micrograph of Fe-Cr-Mn-TiC

3.4 Potentiodynamic Experiments

The potentiodynamic experiments were performed to determine active, active-passive, and passive regions. The experiments were carried out at a scan rate of 2.0 mV/sec. All potentials were measured versus a saturated calomel electrode (SCE). The counter electrode used during the experiments was made of a platinum mesh. The specimens were cleaned by applying a potential of 1V more negative than the free corrosion potential for two minutes before each anodic experiment. The results of potentiodynamic experiments are presented by the polarization curves. An idealized polarization curve for many common solutions is shown in Figure 3-4-1.

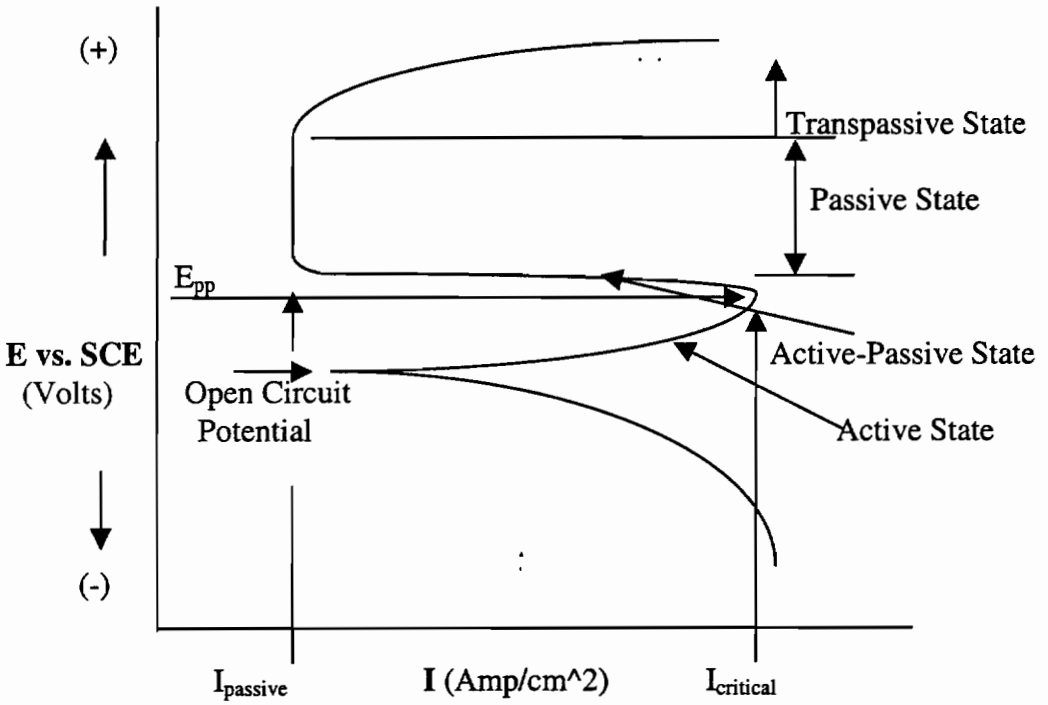

Figure 3-4-1. Idealized Polarization Curve for Many Common Solutions

3.5 Potentiostatic Experiments

The potentiostatic experiments were performed by applying the constant potentials from the active and passive regions. The values of active and passive potentials were determined by using the polarization curves (Figure 3-4-1). A change in current density with time was monitored during the experiments. The experiments were carried out for 15 minutes.

An example of the potentiostatic experiment is shown in Figure 3-5-1. A decreasing in current with time represents the passivation of the material. A current is decreasing linearly means the material is not reaching its true steady state. A slight increase in current or no change in current with time indicates the dissolution of the material.[8]

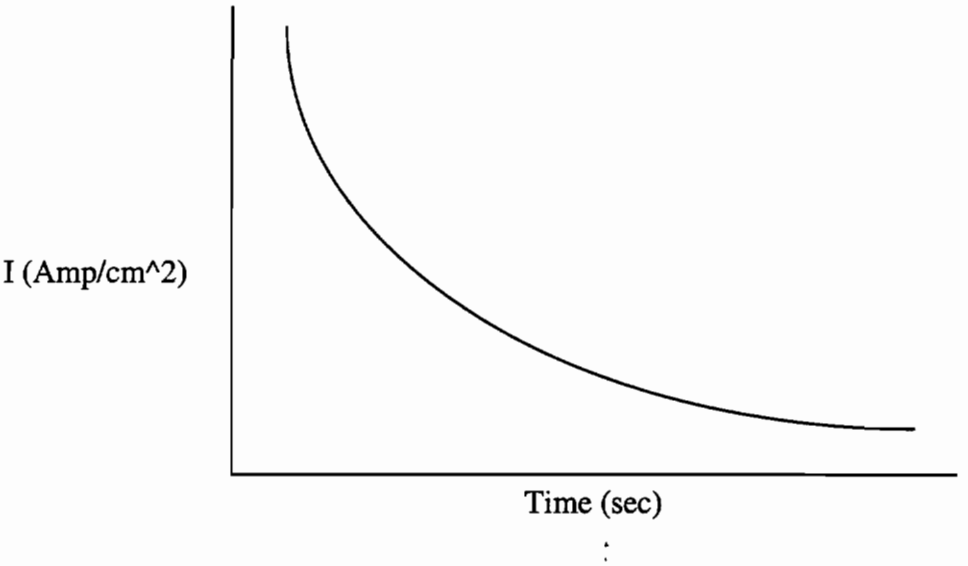

Figure 3-5-1 Result of Potentiostatic Experiment

3.6 Open Circuit Potential

The open circuit potential experiments are used to determine whether or not their current values stay in the active or passive state which are determined in the potentiodynamic experiments. The experiments were carried out for at least 12 hours. An example of open circuit the experiment is shown in Figure 3-6-1.

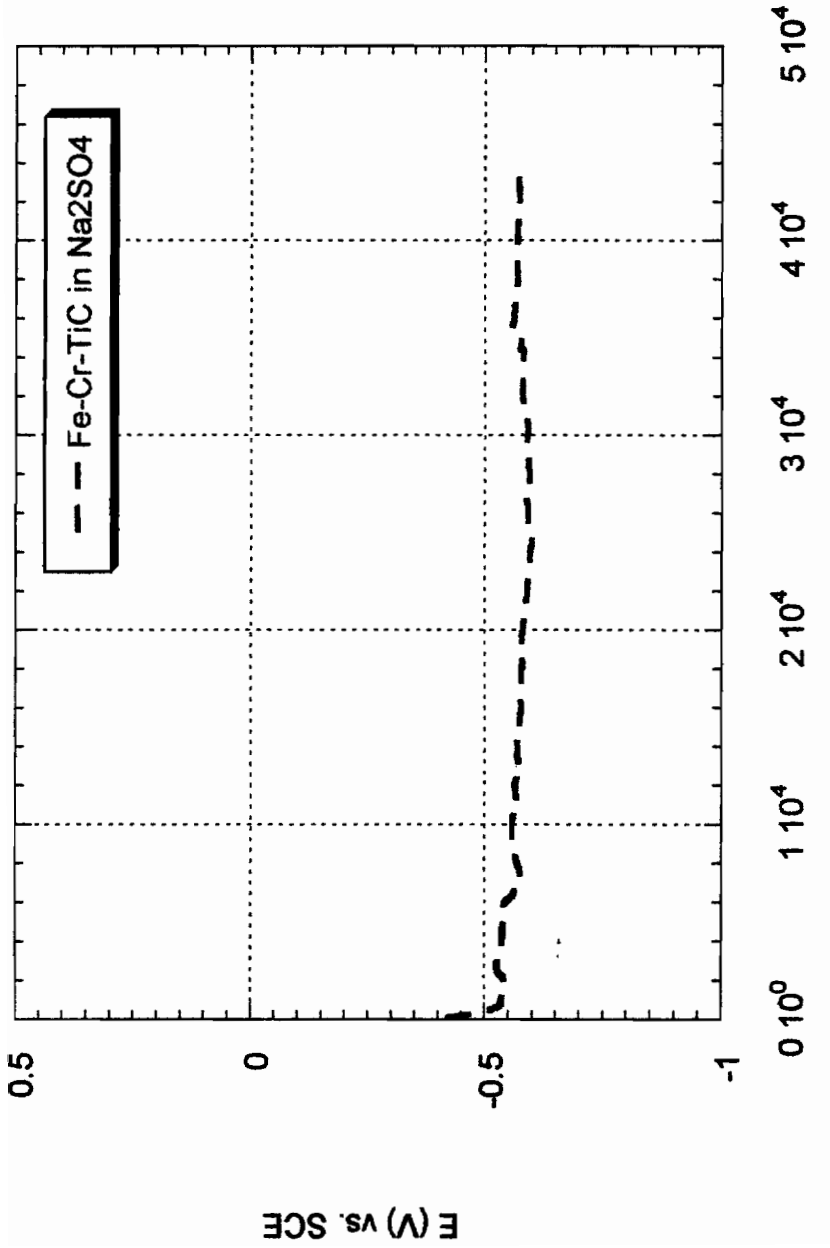

Figure 3-6-1. Result of Open Circuit Potential Experiment

Chapter 4

Results and Discussion

4.1 Effect of Chemical Composition of Composites

4.1.1 Fe-TiC and Fe-Cr-TiC in 1N H_2SO_4

As it is shown in Figure 4-1-1-1, reproducibility of the potentiodynamic experiments is very good.

Figure 4-1-1-2 shows anodic polarization curves for Fe-TiC and Fe-Cr-TiC in 1N sulfuric acid solution. Fe-TiC and Fe-Cr-TiC show active, active-passive, passive and transpassive states. Up to 1V, Fe-TiC exhibits higher current values than Fe-Cr-TiC. The value of the critical passivation current ($I_{critical}$) for Fe-TiC is 3 x 10^{-1} Amp/cm^2 at approximately –0.1 V. The current values stay constant up to 0.3 V forming a plateau similar to the one for iron. The presence of this plateau could be explained by forming a partially insulating film of $FeSO_4$ on the surface of Fe-TiC composite. [11]

For Fe-Cr-TiC, the value of $I_{critical}$ is approximately 3 x 10^{-2} Amp/cm^2 at –0.1 V. The values of the primary passive potential (E_{pp}) for Fe-TiC and Fe-Cr-TiC are approximately the same, but the current values are lower for Fe-Cr-TiC than those for Fe-TiC.

For Fe-TiC, the current value in the passive region is 5 x 10^{-3} Amp/cm^2 at approximately 0.4 V. For Fe-Cr-TiC, the current value is 3 x 10^{-4} Amp/cm^2.

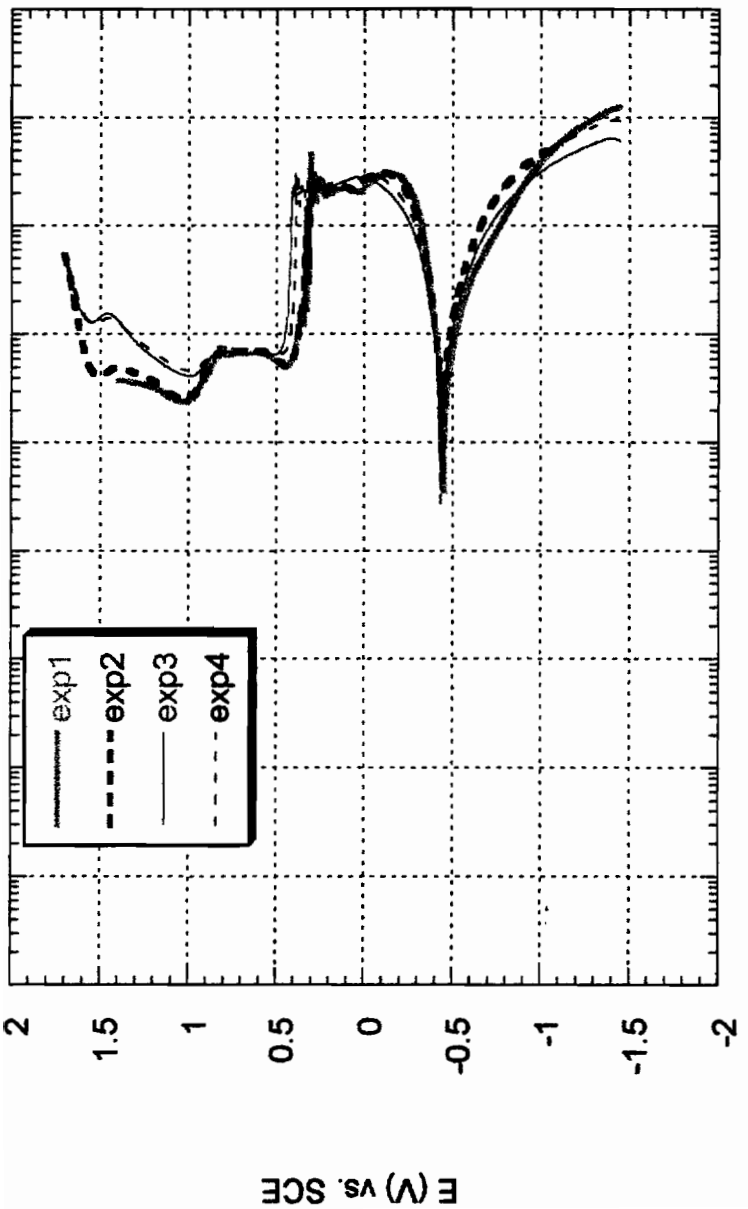

Figure 4-1-1-1. Anodic Polarization Curves for Fe-TiC in H2SO4

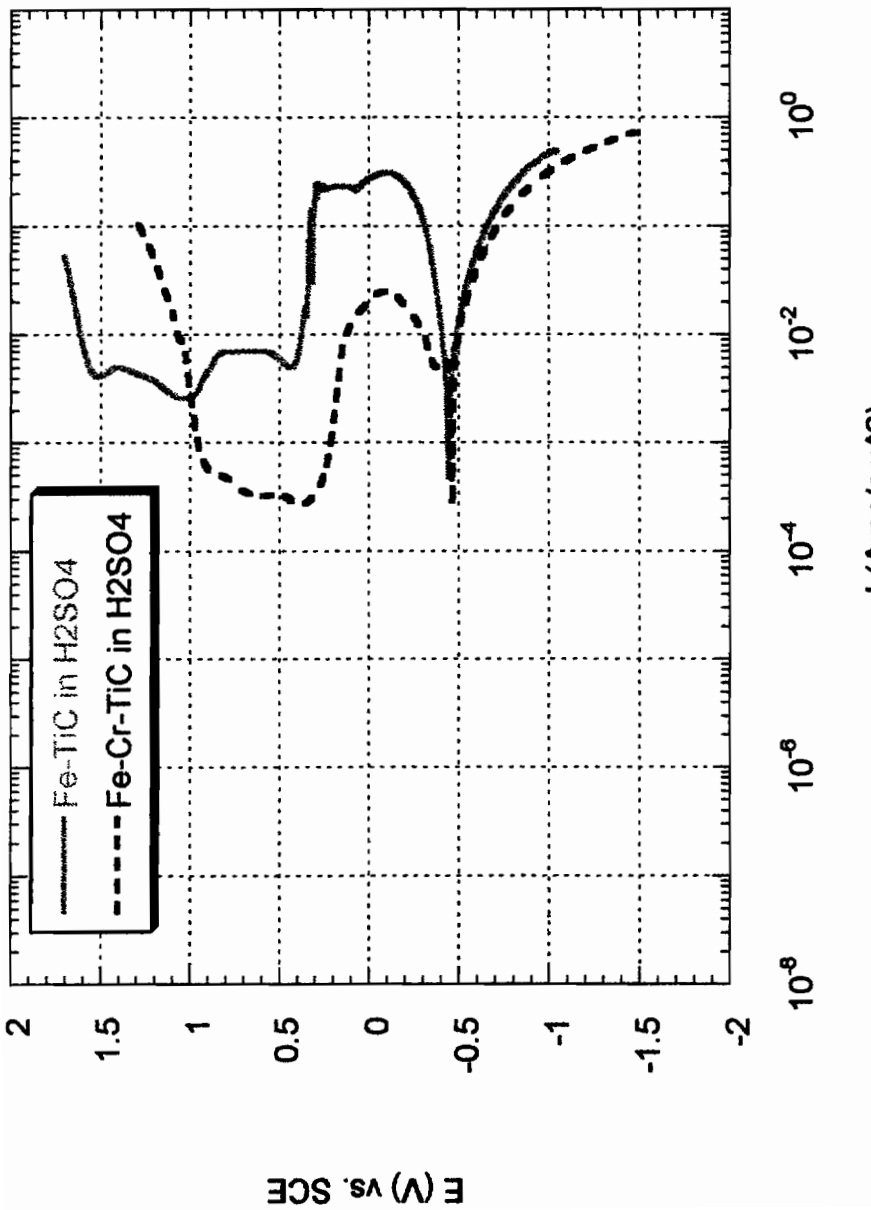

Figure 4-1-1-2. Anodic Polarization Curve for Fe-TiC and Fe-Cr-TiC in 1N H2SO4

For Fe-TiC, the passive region is from 0.4V to 1.5V whereas for Fe-Cr-TiC is from 0.4 V to 0.9 V. This difference in the passive region range could be explained by the Pourbaix diagram for iron superimposed on the Pourbaix diagram for chromium shown in Figure 4-1-1-3. The shaded area indicates the stability of Cr_2O_3 in Figure 4-1-1-3. Figure 4-1-1-3 indicates the following films, Fe_3O_4, Cr_2O_3 and Fe_2O_3.

The literature data also show that the film formed on the surface of Fe-22Cr at +0.5 V in sulfuric acid has 4 to 5 times higher concentration of Cr than the film formed in the air. The oxide layer showed 88 to 95 % Cr and 12 to 50 % Fe depending on the passivation time. [12]

4.1.2 Fe-Cr-TiC and Fe-Cr-Mn-TiC in 1N H_2SO_4

Figure 4-1-2-1 shows anodic polarization curves for Fe-Cr-TiC and Fe-Cr-Mn-TiC in 1N sulfuric acid solution. Both investigated material show the active, active-passive, passive and transpassive states.

At any applied potentials, the current values for Fe-Cr-TiC and Fe-Cr-Mn-TiC are very similar to each other. The value of $I_{critical}$ is approximately 3 x 10^{-2} Amp/cm^2 at –0.1 V for Fe-Cr-TiC and at –0.4 V for Fe-Cr-Mn-TiC. The current value for Fe-Cr-TiC and Fe-Cr-Mn-TiC in the passive region is 3 x 10^{-4} Amp/cm^2 at 0.35 V. For both materials, the transpassive region starts at 0.9 V. This is probably a beneficial effect of chromium.

The shape of the anodic polarization curves for Fe-Cr-TiC and Fe-Cr-Mn-TiC are very similar to each other, but addition of manganese affects the dissolution in the active region. This could be explained by Pourbaix diagram for manganese shown in Figure 4-1-2-2. This diagram indicates a large region of Mn^{++}.

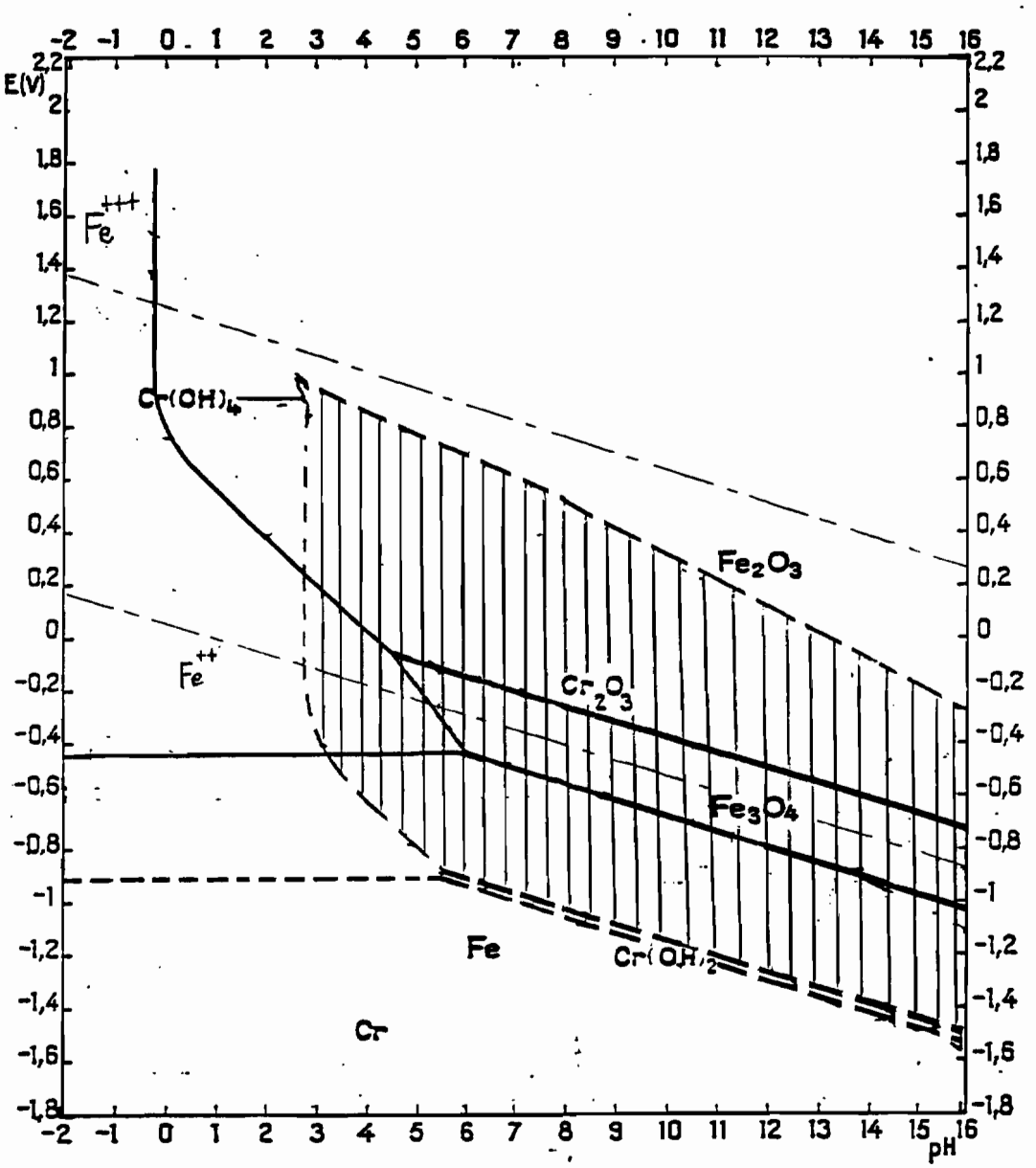

Figure 4-1-1-3. Pourbaix Diagram for Iron superimposed on the Pourbaix Diagram for Chromium

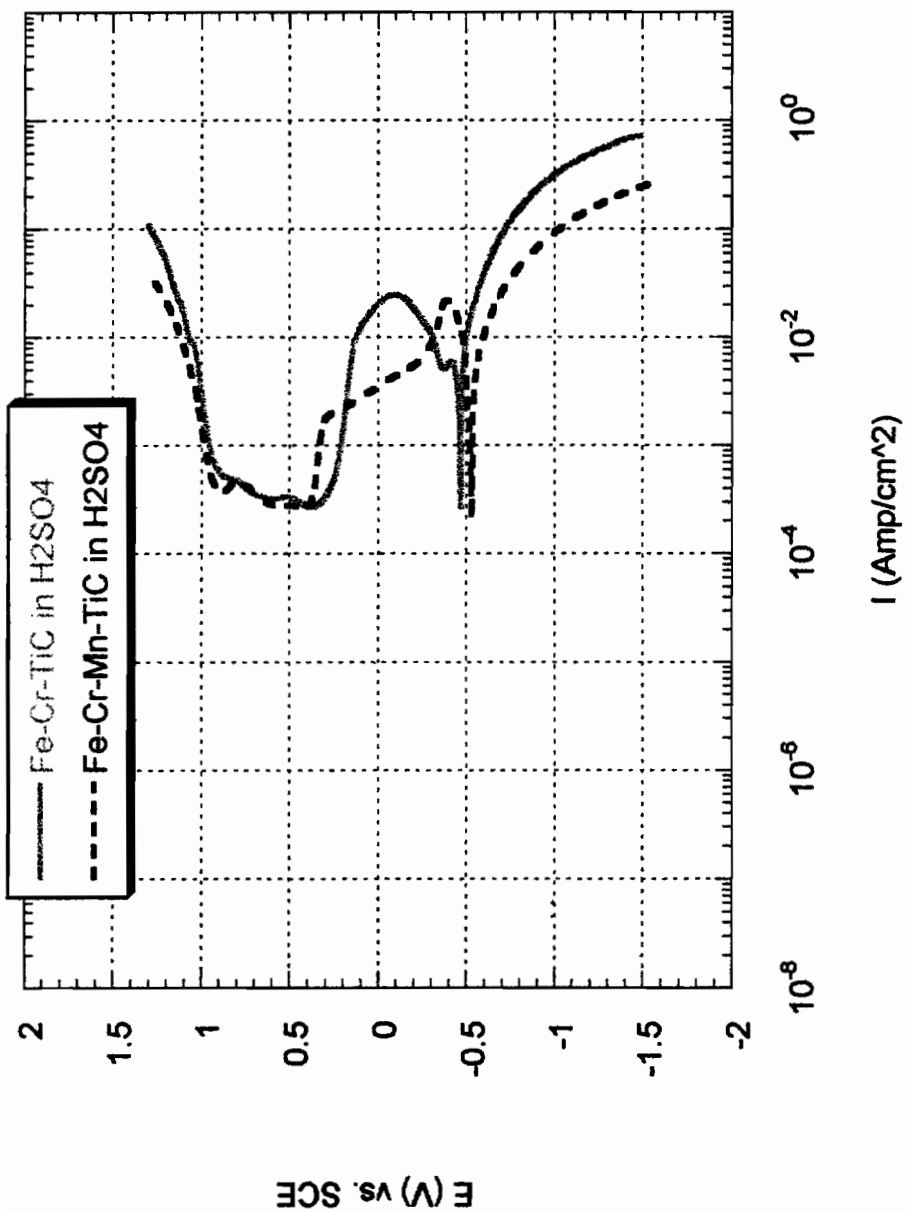

Figure 4-1-2-1. Anodic Polarization Curves for Fe-Cr-TiC and Fe-Cr-Mn-TiC in 1N H2SO4

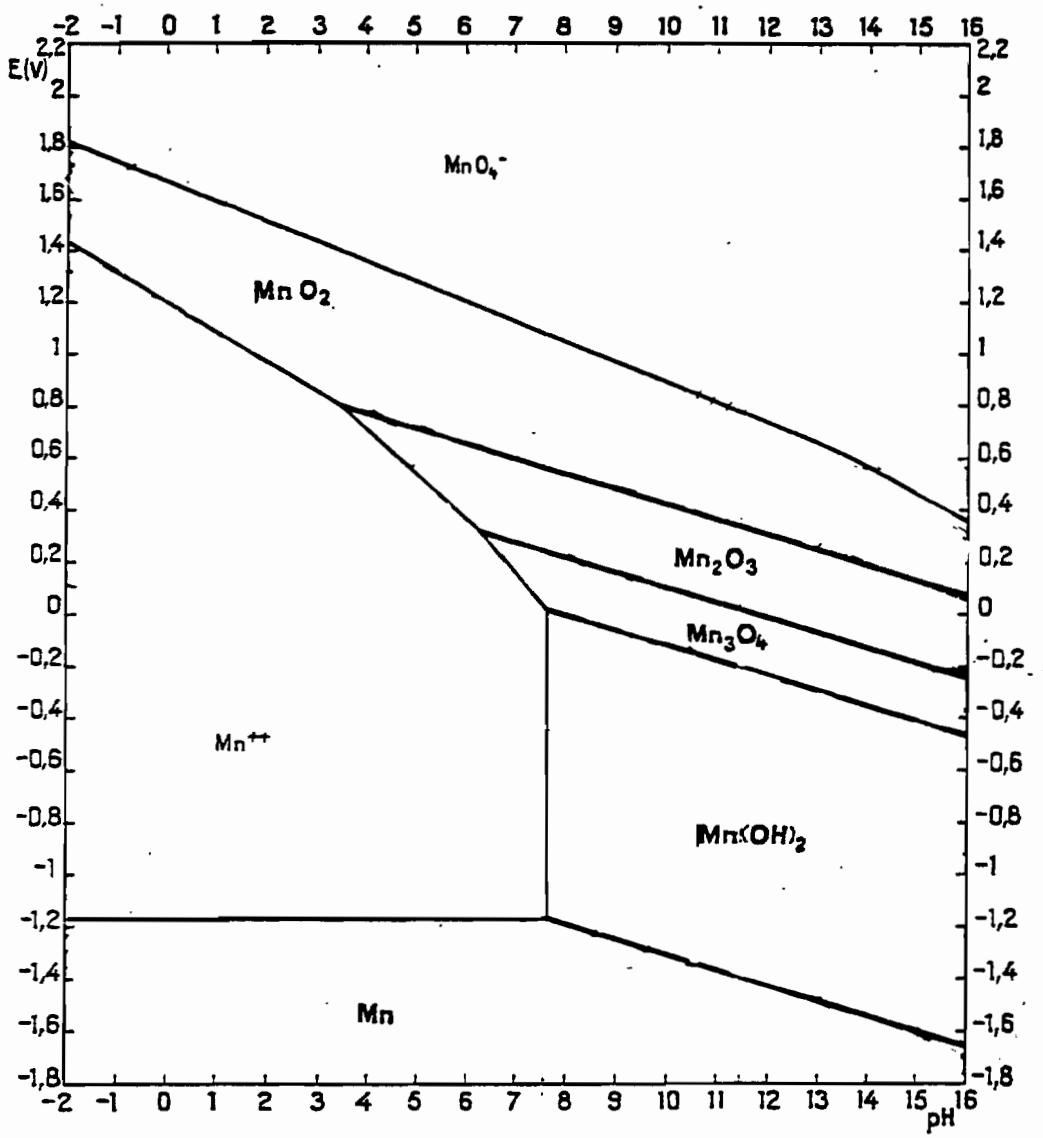

Figure 4-1-2-2. Pourbaix diagram for Manganese

4.1.3 Fe-TiC, Fe-Cr-TiC, Fe-Cr-Mn-TiC and matrix of Fe-TiC in H_2SO_4

Figure 4-1-3-1 shows anodic polarization curves for Fe-TiC, Fe-Cr-TiC, Fe-Cr-Mn-TiC and the matrix of Fe-TiC in the sulfuric acid solution. In the passive region, the matrix of Fe-TiC shows lower current values than Fe-TiC and higher current values than the composites containing the chromium and the manganese. This indicates that the passive film formed on Fe-TiC is less protective than the one formed on the surface of the Fe-TiC matrix.

It is not surprising that the lowest current in the passive region is observed for the composites containing chromium. It is known that chromium increases corrosion resistance of steel. In the active region, Fe-TiC and the matrix of Fe-TiC is very similar to each other. They both show a plateau similar to the one observed for iron in H_2SO_4. However, the composites containing the chromium and the manganese show lower $I_{critical}$ than Fe-TiC and the Fe-TiC matrix.

4.1.4 Fe-TiC and Fe-Cr-TiC in 1N Na_2SO_4

Figure 4-1-4-1 shows anodic polarization curves for Fe-TiC and Fe-Cr-TiC in the 1N sodium sulfate solution. Both materials show active, active-passive, passive and transpassive states.

Up to a potential of 1V, Fe-Cr-TiC shows lower current values than Fe-TiC. The Fe-Cr-TiC composite reaches $I_{critical}$ of 3×10^{-3} Amp/cm^2 at 0.0 V. The current values in the passive region are approximately 6×10^{-5} Amp/cm^2 and the passive region begins at 0.3 V.

Fe-TiC reaches its $I_{critical}$ of approximately 3×10^{-1} Amp/cm^2 at –0.3 V. The current values in the passive region are approximately 10^{-2} Amp/cm^2 at 0.3 V.

The literature data indicate that for Fe-23Cr, Cr in the oxide film is primarily Cr^{3+} in an acidic solution with pH of 4.5. In this solution, the film formed at the beginning of the passive region contains to 100 % Cr and at the end of the passive region the Cr concentration is decreases to 50 %. [12]

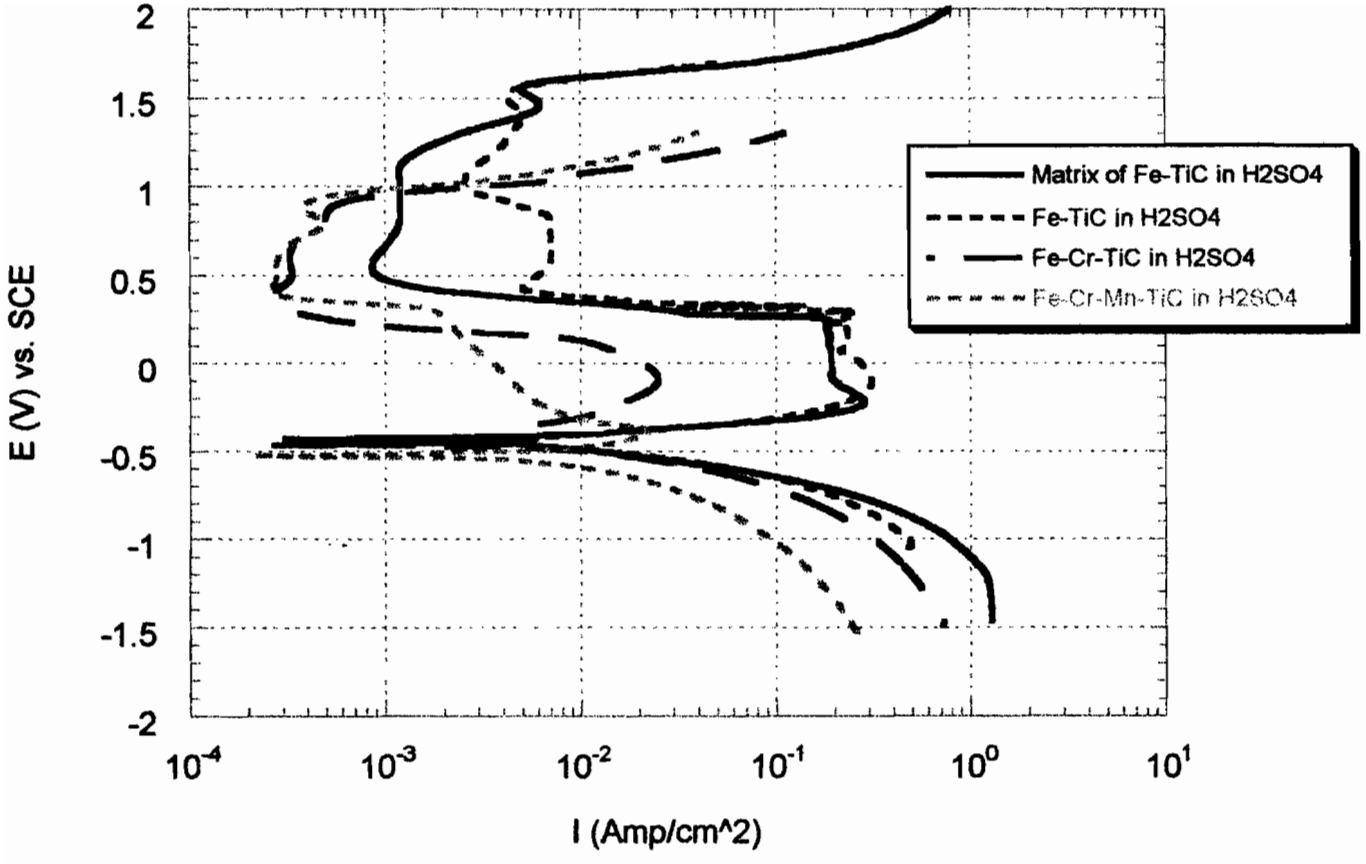

Figure 4-1-3-1. Anodic Polarization Curves for Fe-TiC, Fe-Cr-TiC, Fe-Cr-Mn-TiC and Matrix of Fe-TiC in H2SO4

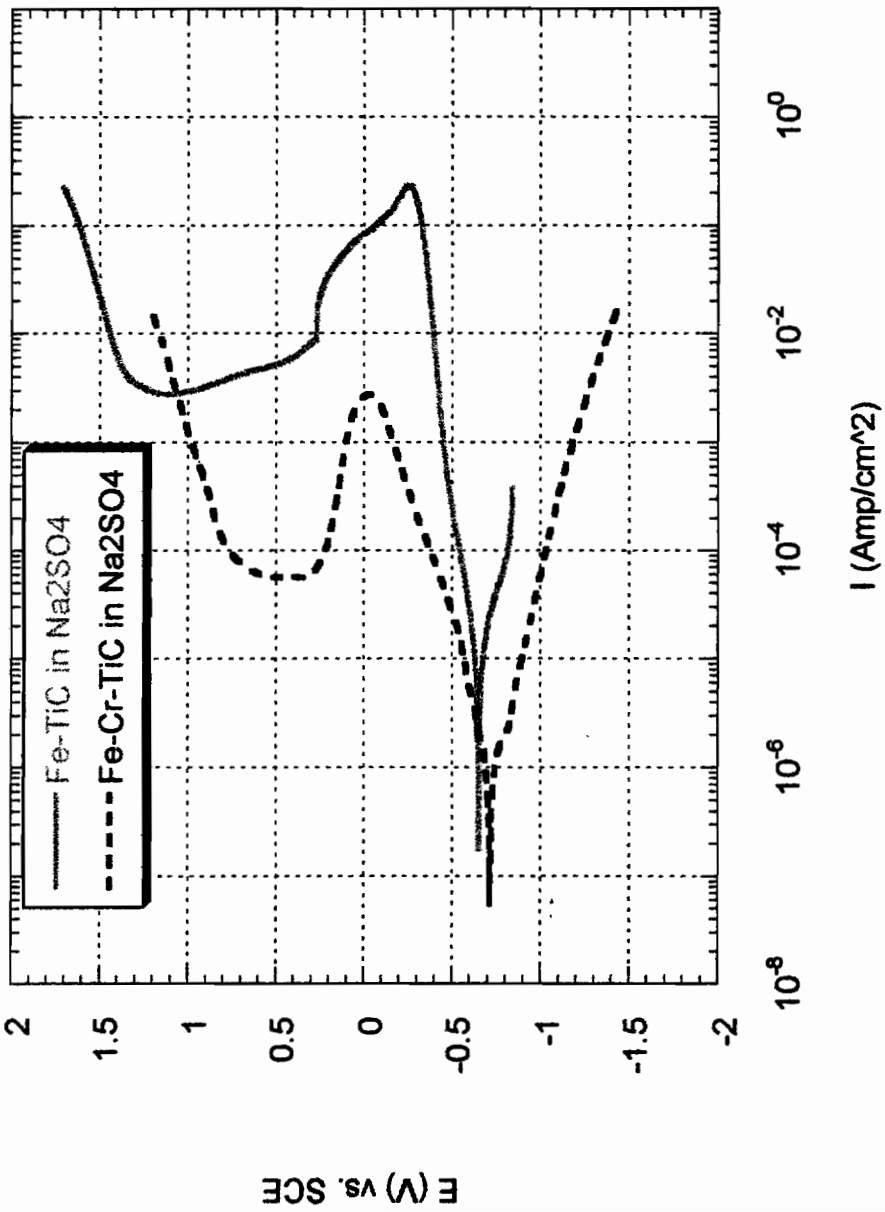

Figure 4-1-4-1. Anodic Polarization Curves for Fe-TiC and Fe-Cr-TiC in 1N Na2SO4

4-1-5. Fe-Cr-TiC and Fe-Cr-Mn-TiC in 1N Na_2SO_4

The shape of the anodic polarization curves for Fe-Cr-TiC and Fe-Cr-Mn-TiC in the 1N sodium sulfate solution are different from each other (Figure 4-1-5-1). However, both investigated materials show active, active-passive, passive, and transpassive regions.

Fe-Cr-TiC reaches $I_{critical}$ of 3 x 10^{-3} Amp/cm^2 at 0.0 V. The current in the passive region starts at 6 x 10^{-5} Amp/cm^2 and at the potential value of 0.3 V. The transpassive state begins at approximately 0.75 V.

Fe-Cr-Mn-TiC reaches $I_{critical}$ value of approximately 3 x 10^{-4} Amp/cm^2 at approximately -0.1 V. This value is almost constant up to 0.3 V. At 0.4 V, current drops to approximately 7 x 10^{-5} Amp/cm^2. The transpassive state starts at 0.8 V.

The open circuit potential for Fe-Cr-TiC is slightly higher than that for Fe-Cr-Mn-TiC. The current values for Fe-Cr-TiC and Fe-Cr-Mn-TiC in the passive region are very similar to each other. The value of the primary passive potential (E_{pp}) is approximately the same for both materials; however, Fe-Cr-Mn-TiC shows lower $I_{critical}$.

4-1-6. Fe-TiC, Fe-Cr-TiC, Fe-Cr-Mn-TiC and Fe-TiC matrix in Na_2SO_4

Figure 4-1-6-1 shows anodic polarization curves for Fe-TiC, Fe-Cr-TiC, Fe-Cr-Mn-TiC and the Fe-TiC matrix in the sodium sulfate solution. The lowest $I_{critical}$ is observed for Fe-Cr-Mn-TiC. In the passive region, Fe-Cr-TiC and Fe-Cr-Mn-TiC show similar current values. Similar $I_{critical}$ values are observed for Fe-TiC and the matrix of Fe-TiC. Similar to the results observed in the sulfuric acid solution, the film formed on Fe-TiC is less protective than the one formed on the matrix of Fe-TiC.

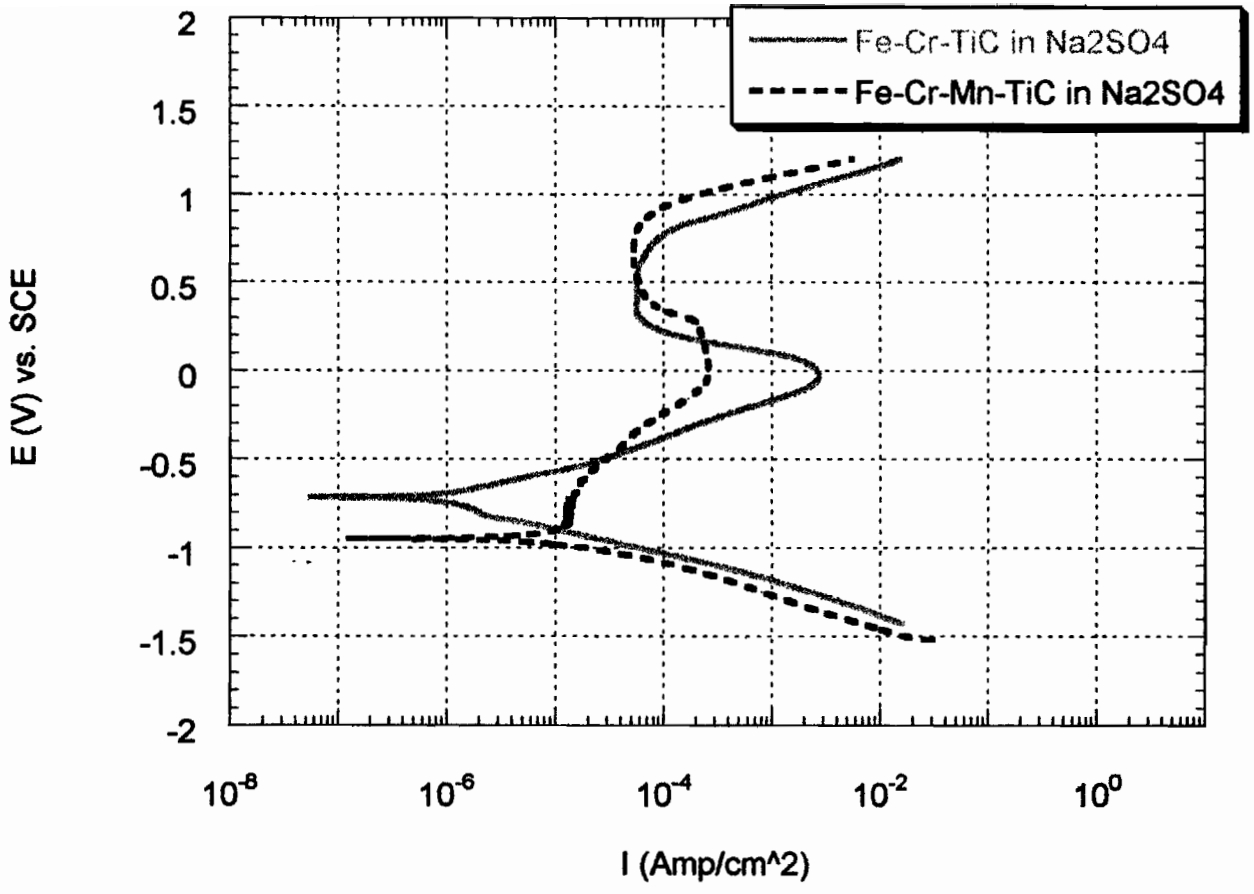

Figure 4-1-5-1. Anodic Polarization Curves for Fe-Cr-TiC and Fe-Cr-Mn-TiC in 1N Na2SO4

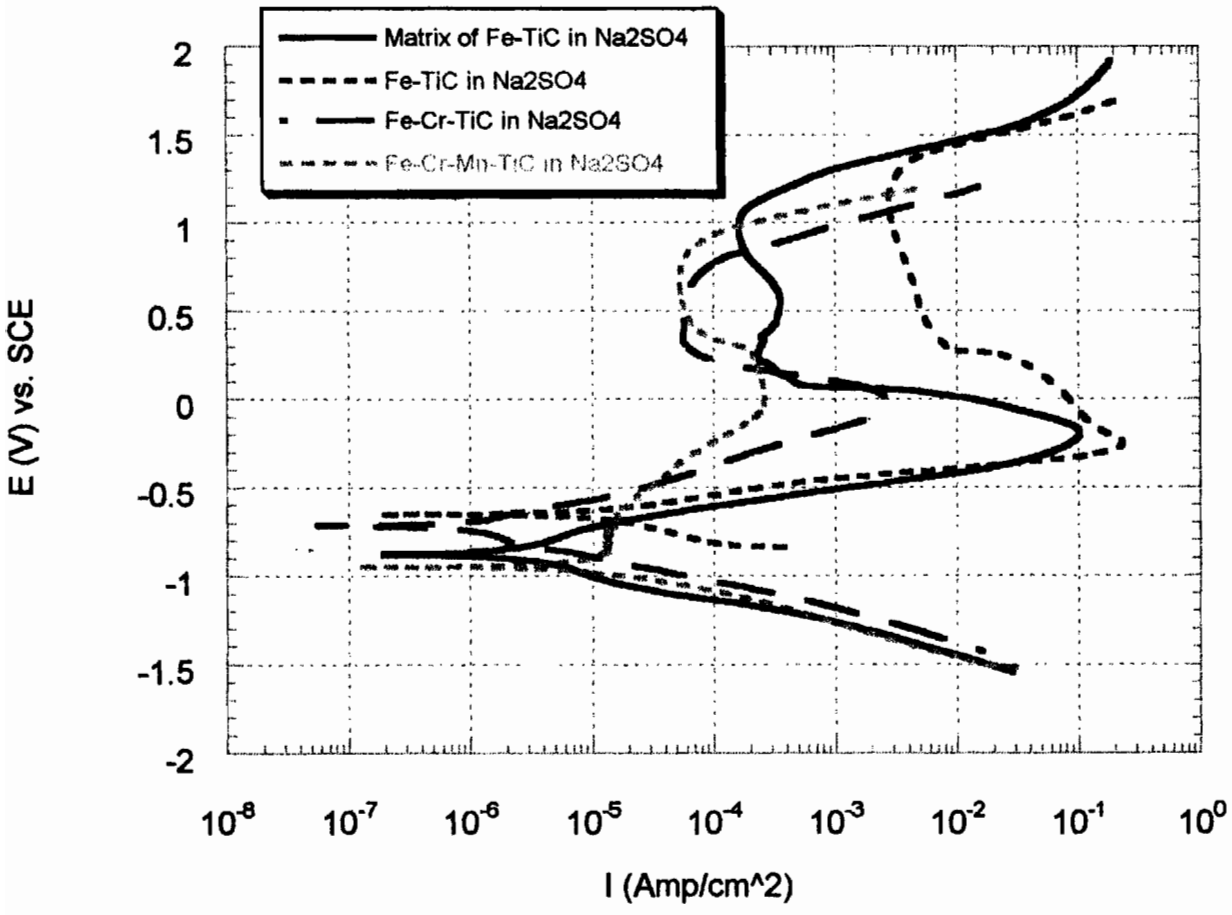

Figure 4-1-6-1. Anodic Polarization Curves for Fe-TiC, Fe-Cr-TiC, Fe-Cr-Mn-TiC and Matrix of Fe-TiC in Na2SO4

4.2 Effect of TiC

4-2-1. Fe-TiC and Matrix of Fe-TiC

Figure 4-2-1-1 shows anodic polarization curves for Fe-TiC and the matrix of Fe-TiC in 1N H_2SO_4. The shape of the polarization curves for both materials are very similar to each other. The passive regions for both materials are between approximately 0.4 V and 1.6 V, but the current values in the passive region are different. The current value for the matrix of Fe-TiC in the passive region is lower than that for Fe-TiC. This indicates that the film for the composite is less protective than that for the matrix, and the properties of the passive films are different. They both showed plateau similar to the one observed for iron.

Figure 4-2-1-2 show anodic polarization curves for Fe-TiC and the matrix of Fe-TiC in 1N Na_2SO_4. In the passive region, the matrix of Fe-TiC shows lower current densities than Fe-TiC. For both materials, the potential values of E_{pp} and the passive region are very similar to each other. The current value of $I_{critical}$ for Fe-TiC is 3×10^{-1} Amp/cm^2 and for the matrix of Fe-TiC is 10^{-1} Amp/cm^2. The value of current in the passive region for the matrix of Fe-TiC is approximately 2×10^{-4} Amp/cm^2, and the value of current in the passive region for Fe-TiC is 10^{-2} Amp/cm^2. This indicates that, the addition of TiC probably activates the substrate in the passive region.

4-2-2. Fe-Cr-TiC and Matrix of Fe-Cr-TiC

Figure 4-2-2-1 show anodic polarization curves for Fe-Cr-TiC and the matrix of Fe-Cr-TiC in 1N H_2SO_4. The different current densities are observed in the active and active-passive regions. This is probably caused by the addition of TiC that activates the substrate in the active and active-passive regions. The $I_{critical}$ is 3×10^{-2} Amp/cm^2 at – 0.1 V for Fe-Cr-TiC and 10^{-2} Amp/cm^2 at – 0.4 V for the matrix of Fe-Cr-TiC. The values of the current densities in the passive region are approximately the same. The transpassive region is reached at the same value of potential and current density.

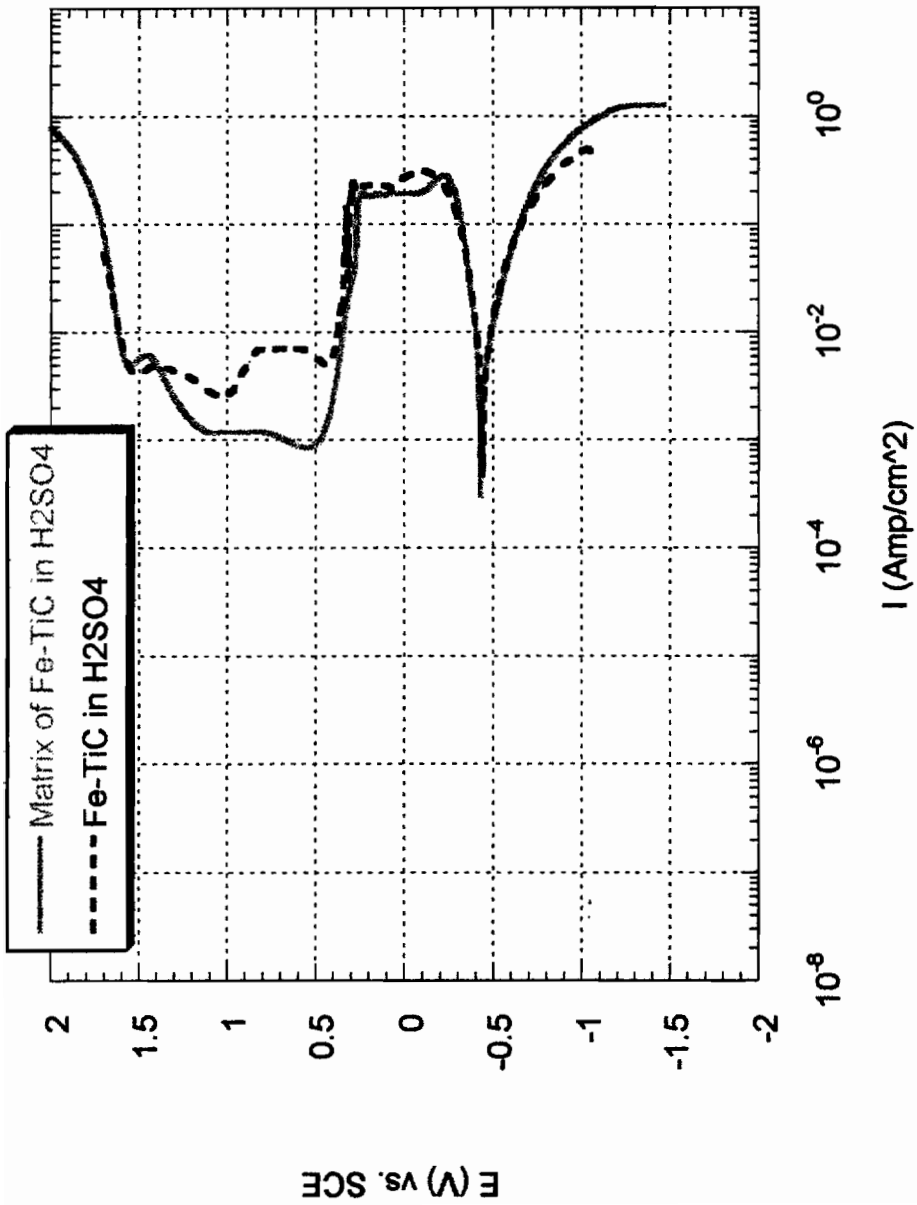

Figure 4-2-1-1. Anodic Polarization Curves for Fe-TiC and Matrix of Fe-TiC in 1N H2SO4

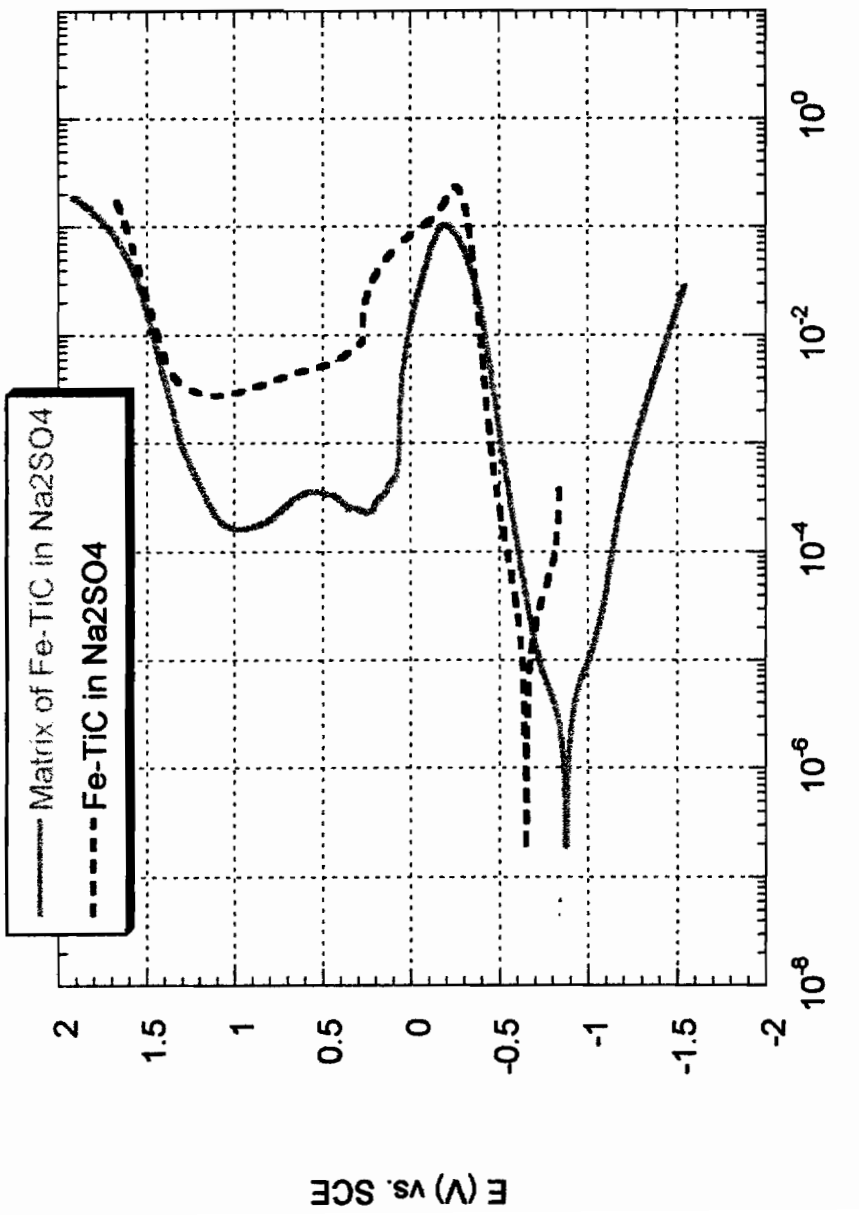

Figure 4-2-1-2. Anodic Polarization Curves for Fe-TiC and Matrix of Fe-TiC in 1N Na2SO4

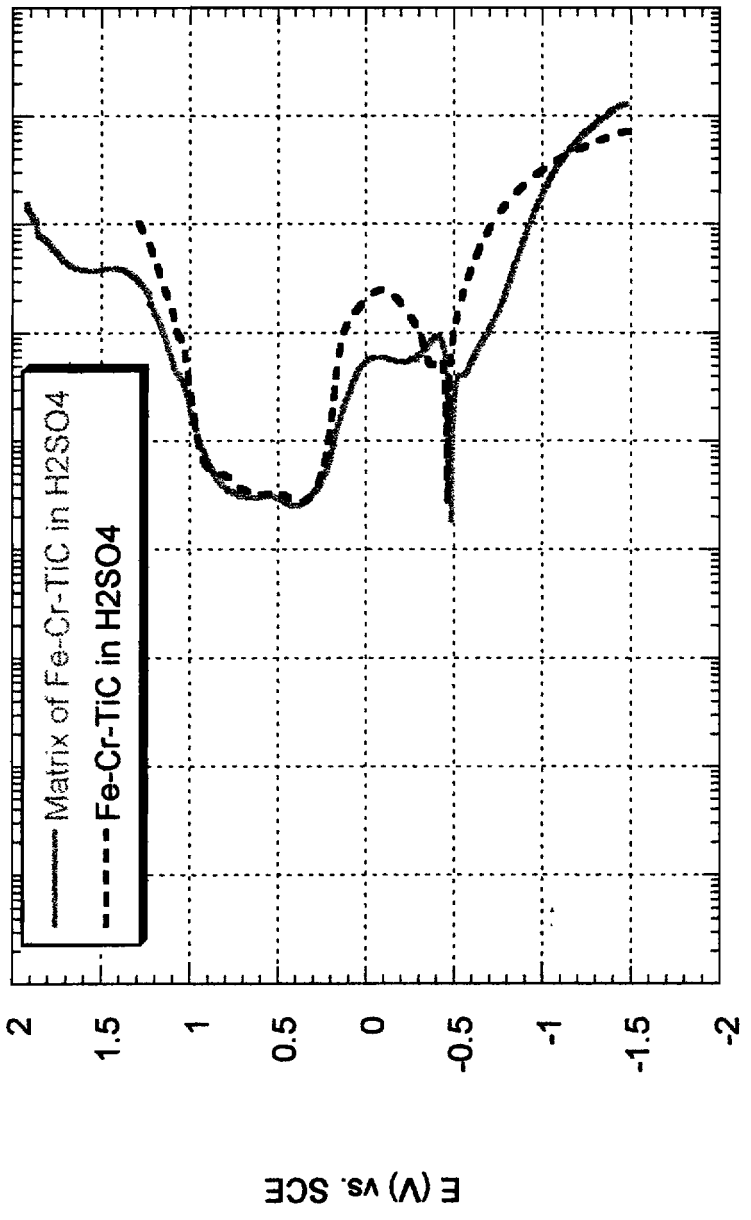

Figure 4-2-2-1. Anodic Polarization Curves for Fe-Cr-TiC and Matrix of Fe-Cr-TiC in 1N H2SO4

Figure 4-2-2-2 shows the anodic polarization curves for the matrix of Fe-Cr-TiC and Fe-Cr-TiC in 1N Na_2SO_4. The shapes of the anodic polarization curves for the matrix of Fe-Cr-TiC and Fe-Cr-TiC are very different from each other in this solution. For the matrix of Fe-Cr-TiC, the value of $I_{critical}$ is 6×10^{-4} Amp/cm^2 at 0.0 V and the value of the current density in the passive region is 3×10^{-3} Amp/cm^2 at 0.0 V. For the matrix of Fe-Cr-TiC, the current values in the passive region and $I_{critical}$ are very close.

4-2-3. Fe-Cr-Mn-TiC and Matrix of Fe-Cr-Mn-TiC

Figure 4-2-3-1 shows the anodic polarization curves for Fe-Cr-Mn-TiC and the matrix of Fe-Cr-Mn-TiC in 1N H_2SO_4. The value of $I_{critical}$ for Fe-Cr-Mn-TiC is 3×10^{-2} Amp/cm^2 at approximately – 0.4 V and for the matrix of Fe-Cr-Mn-TiC is 9×10^{-2} Amp/cm^2 at approximately – 0.4 V. The current value in the passive region is 3×10^{-4} Amp/cm^2 at approximately 0.35 V for Fe-Cr-Mn-TiC, and approximately 10^{-4} Amp/cm^2 at – 0.1 V for the matrix of Fe-Cr-Mn-TiC. The passive region for the matrix of Fe-Cr-Mn-TiC is from –0.1 V to approximately 0.9 V. The passive region for Fe-Cr-Mn-TiC is from 0.35 V to 0.9 V.

Figure 4-2-3-2 shows the anodic polarization curves for Fe-Cr-Mn-TiC and the matrix of Fe-Cr-Mn-TiC in 1N Na_2SO_4. The matrix of Fe-Cr-Mn-TiC shows the passive behavior.

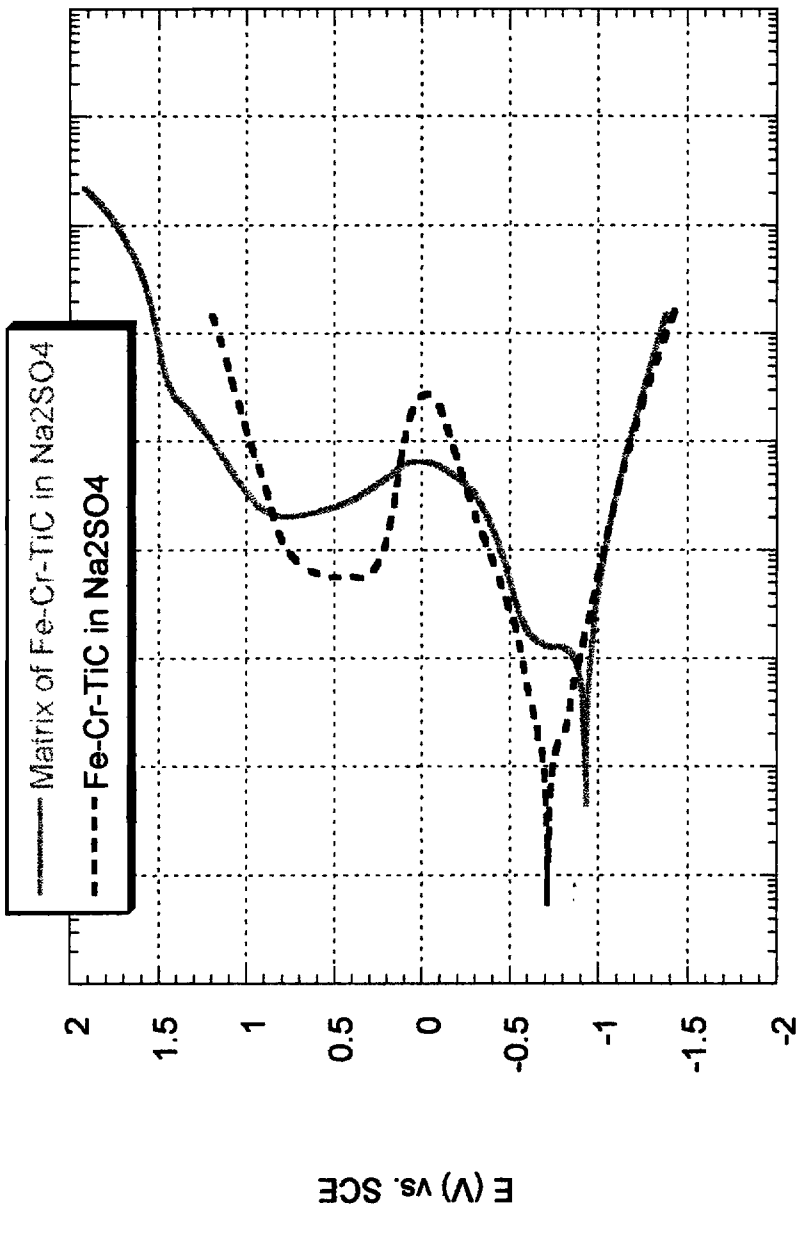

Figure 4-2-2-2. Anodic Polarization Curves for Fe-Cr-TiC and Matrix of Fe-Cr-TiC in 1N Na2SO4

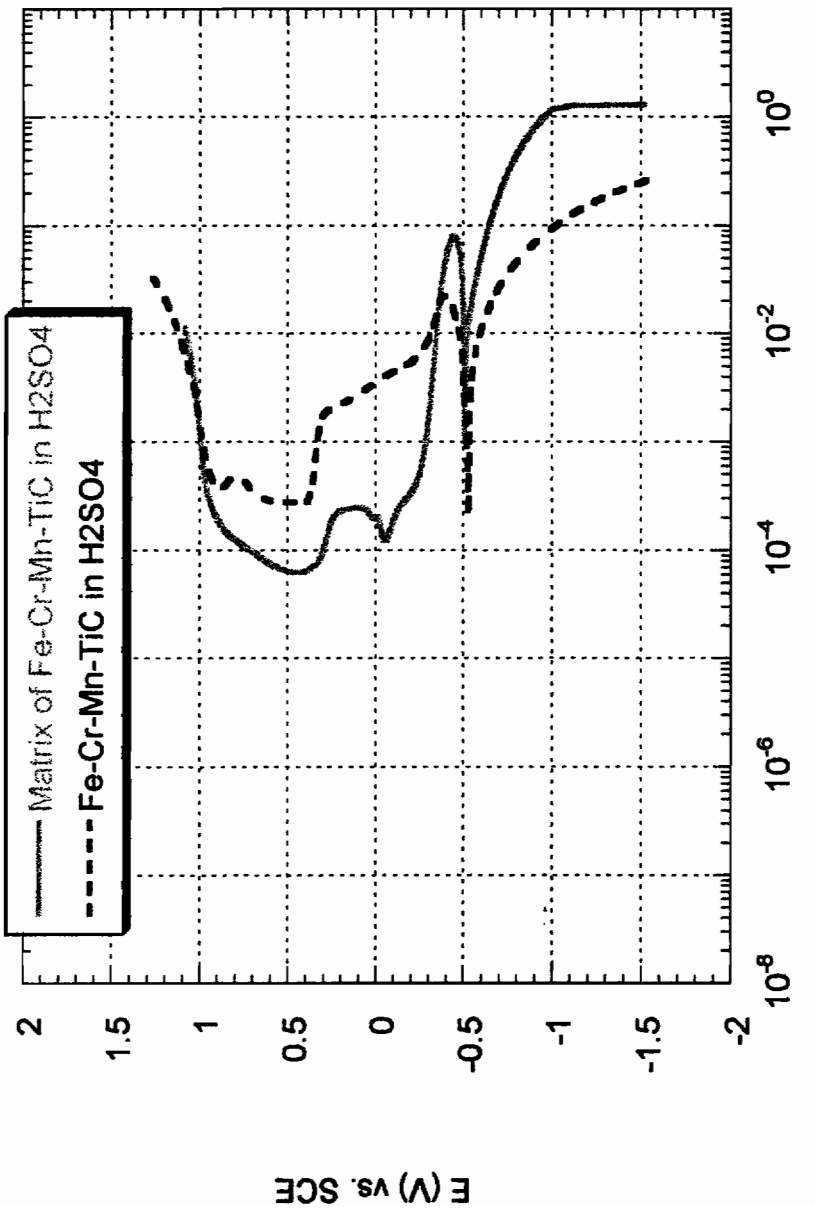

Figure 4-2-3-1. Anodic Polarization Curves for Fe-Cr-Mn-TiC and Matrix of Fe-Cr-Mn-TiC in 1N H2SO4

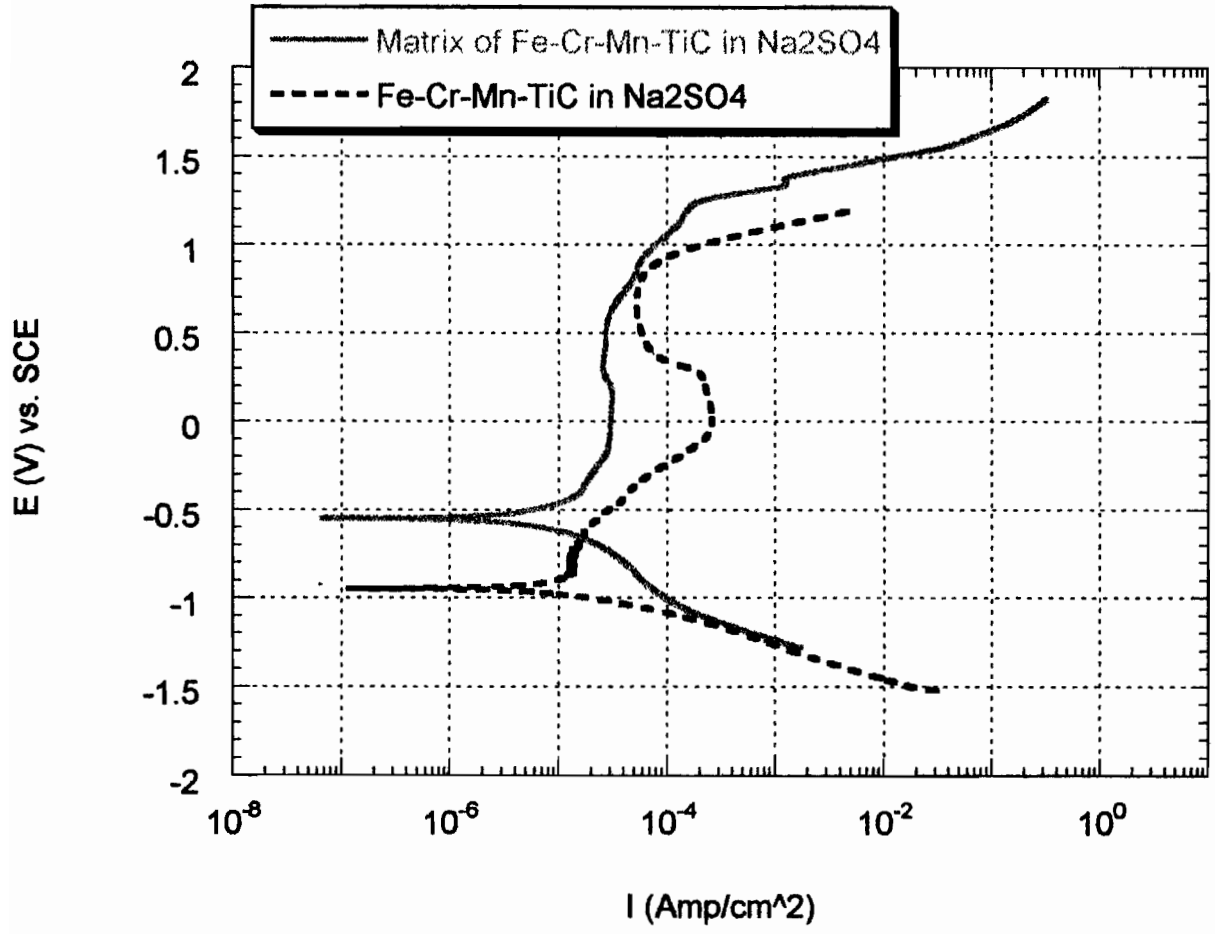

Figure 4-2-3-2. Anodic Polarization Curves for Fe-Cr-Mn-TiC and Matrix of Fe-Cr-Mn-TiC in 1N Na2SO4

4.3 Effect of Chemical Composition of Solutions

4-3-1. Fe-TiC

Figure 4-3-1-1 show anodic polarization curves for Fe-TiC in 1N sulfuric acid and 1N sodium sulfate. In both solutions, Fe-TiC shows active, active-passive, passive and transpassive behavior. In both solutions, the current values for this investigated material are very similar. The pH of the solution does not have much influence on this material; however, it shows two peaks in the passive region and the plateau similar to the one for iron in the sulfuric acid solution. In addition to that, Fe-TiC shows wider active state range in the sodium sulfate solution than that in the sulfuric acid solution. For Fe-TiC in H_2SO_4, the transpassive state starts at 1.5 V whereas in Na_2SO_4 at 1.3 V.

4-3-2. Fe-Cr-TiC

Figure 4-3-2-1 show anodic polarization curves for Fe-Cr-TiC in 1N sulfuric acid and 1N sodium sulfate. In both solutions, Fe-Cr-TiC shows active, active-passive, passive and transpassive states. The shapes of the anodic polarization curves are very similar to each other in both solutions. At any applied potentials, current is higher in the sulfuric acid solution than in the sodium sulfate solution. This indicates higher activity of Fe-Cr-TiC in low pH solution. This result is supported by Pourbaix diagram for iron and chromium (Figure 4-1-1-3). It shows the dissolution process at low pH solution and passive in neutral solution.

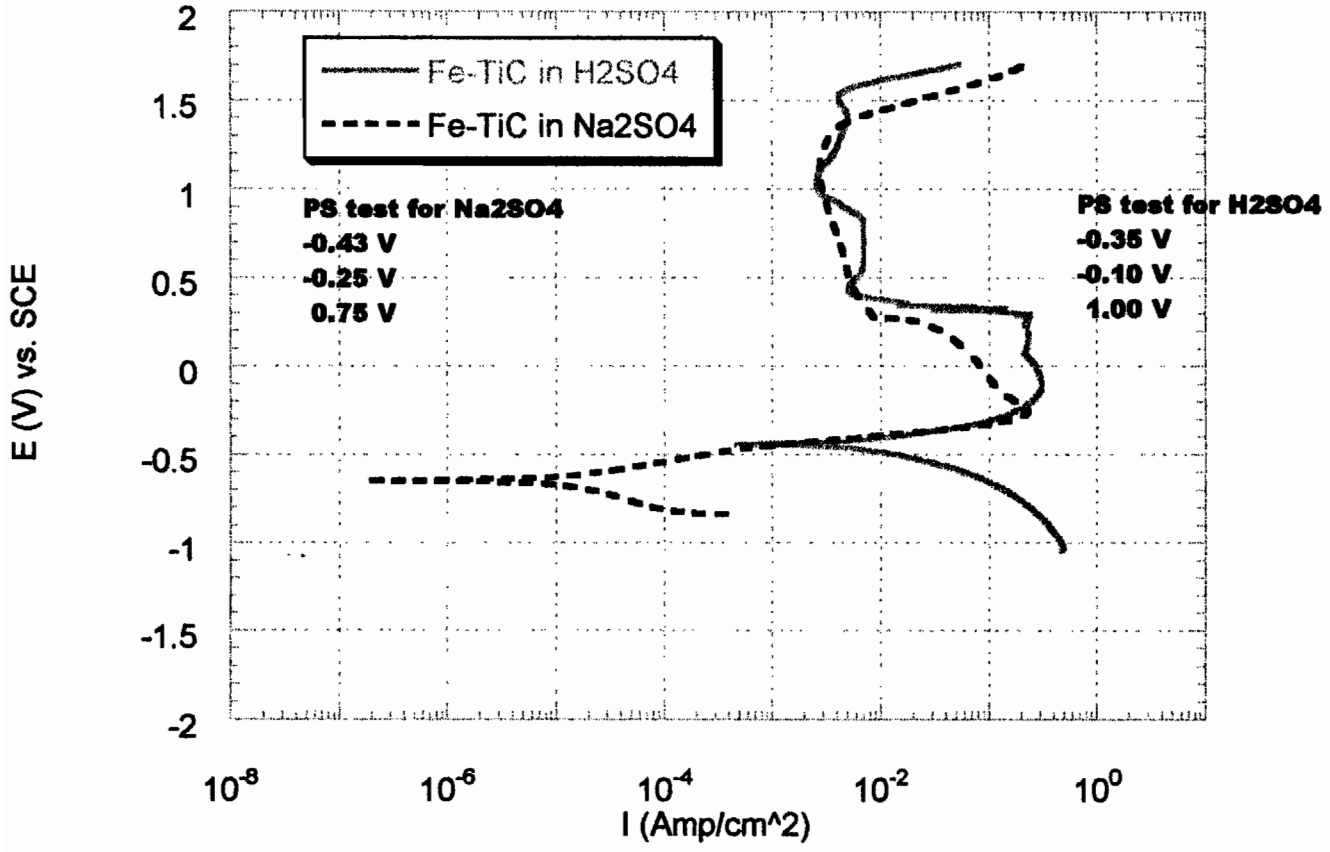

Figure 4-3-1-1. Anodic Polarization Curves for Fe-TiC in H2SO4 and Na2SO4

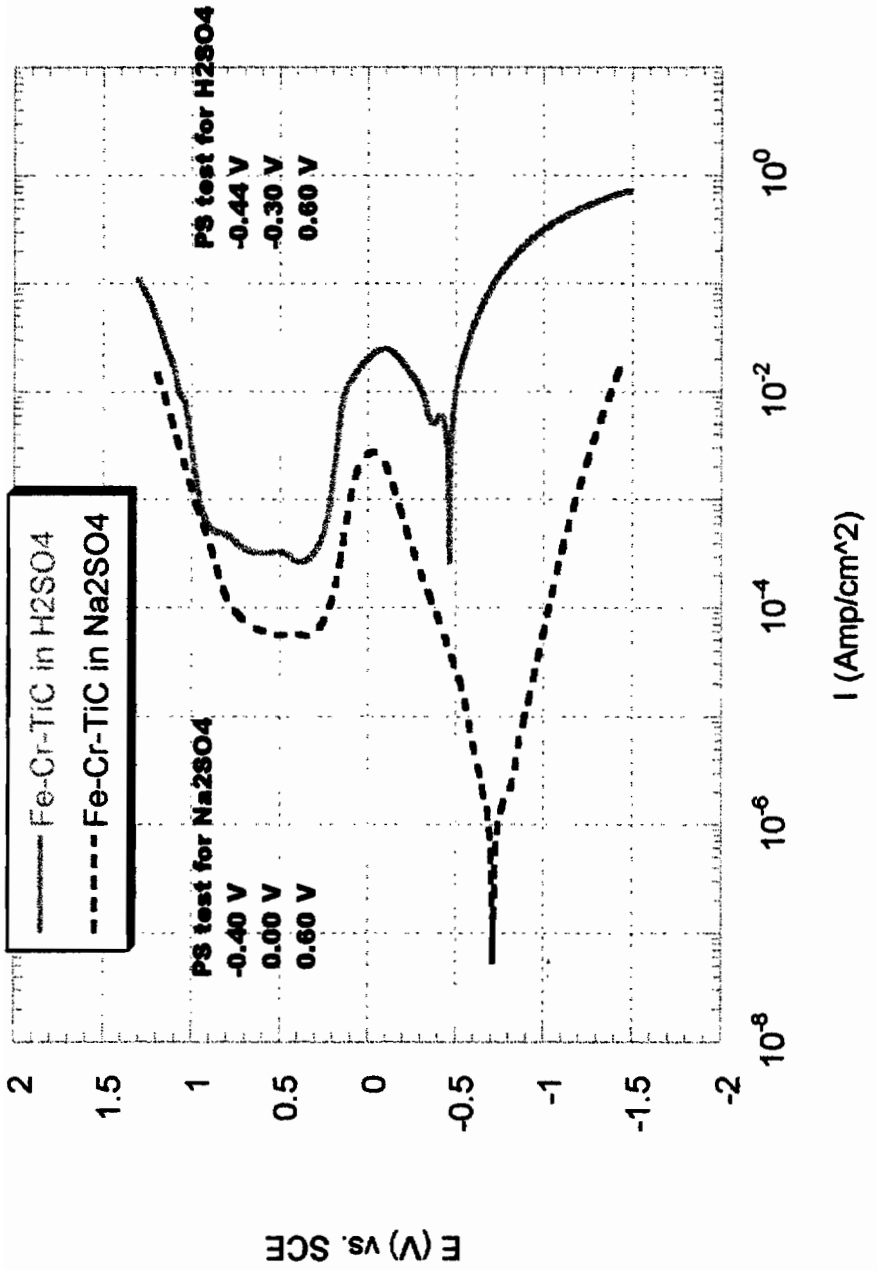

Figure 4-3-2-1. Anodic Polarization Curves for Fe-Cr-TiC in H2SO4 and Na2SO4

4-3-3. Fe-Cr-Mn-TiC

Figure 4-3-3-1 shows the anodic polarization curves for Fe-Cr-Mn-TiC in 1N sulfuric acid and 1N sodium sulfate. This material also shows active, active-passive, passive and transpassive states in both solutions. At any applied potential, the current is higher in the sulfuric acid solution than in the sodium sulfate solution. Indicating higher activity of Fe-Cr-Mn-TiC in the H_2SO_4 solution.

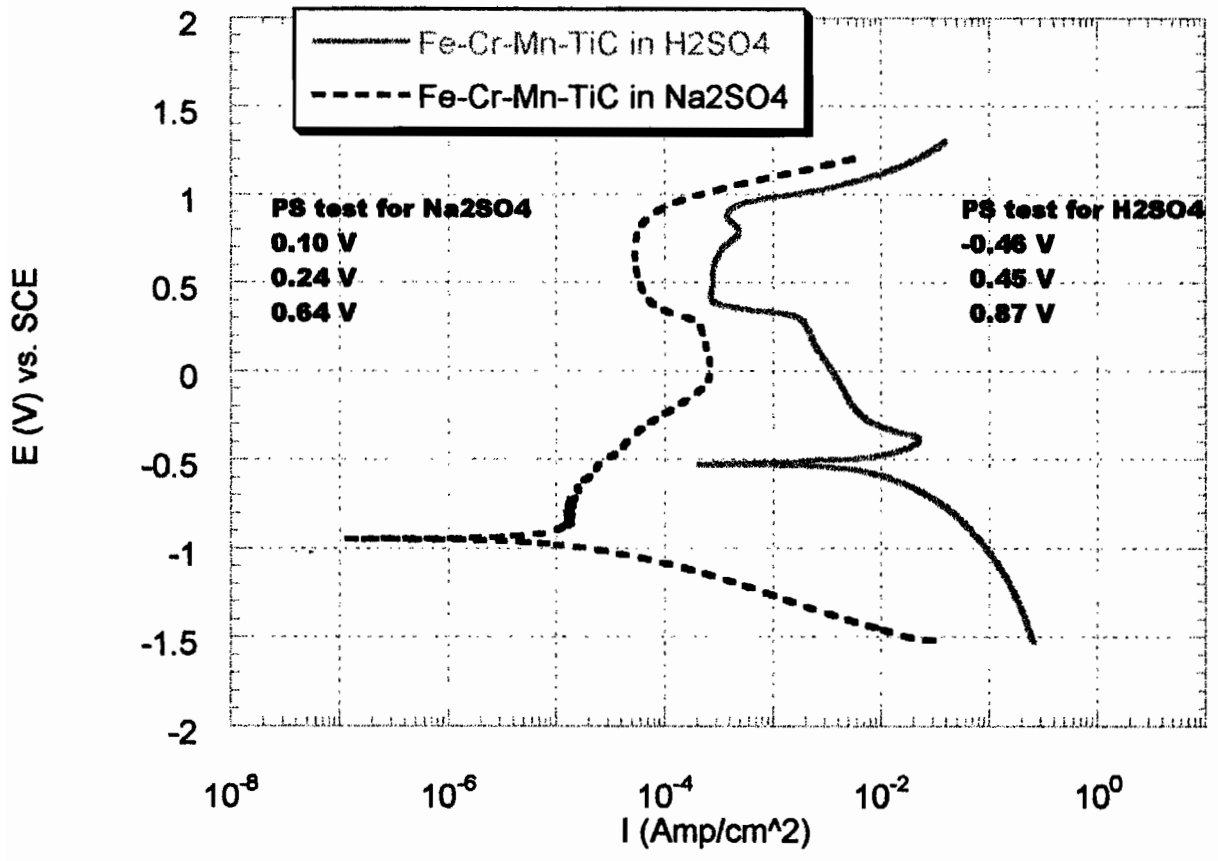

Figure 4-3-3-1. Anodic Polarization Curves for Fe-Cr-Mn-TiC in H2SO4 and Na2SO4

4.4 Potentiostatic Experiments

Figure 4-4-1 shows the result of the potentiostatic experiment for Fe-TiC in the sulfuric acid solution. The highest current value is observed for the potential value of -0.1V at the critical passivation current. This curve represents the dissolution of the material. The second highest current value is observed at the potential value of -0.35V in the active region. This line also represents the dissolution of the material. The lowest current value is observed at the potential value of 1.0V in the passive region. This curve represents the passivation of the material. The results agree with the polarization curve for Fe-TiC in the sulfuric acid solution.

Figure 4-4-2 shows the current-time curves for Fe-TiC in the sodium sulfate solution. The highest current value is observed at the potential value of -0.25V at the critical passivation current. The second highest current value of -0.43V is observed in the active region. Both curves represent the dissolution of the material. The lowest current value at 0.75V is observed in the passive region. This curve represents the passivation of the material. The results agree with the polarization curves for Fe-TiC in the sodium sulfate solution.

Figure 4-4-3 shows the result of the potentiostatic experiment for Fe-Cr-TiC in the sulfuric acid solution. The highest current is observed for the E_{pp} potential of -0.3V. Slightly lower current is observed at the applied potential value of -0.44V in the active region. The lowest current values are observed at the applied potential value of 0.6V in the passive region. Again, these results agree with the polarization curve for Fe-Cr-TiC in sulfuric acid.

Figure 4-4-4 shows the results of the potentiostatic experiment for Fe-Cr-TiC in the sodium sulfate solution. As expected from the polarization curve for Fe-Cr-TiC in the sodium sulfate solution, the highest current values are observed at the E_{pp} potential of 0.0V. Slightly lower current is observed at the applied potential in the active region (-0.4V). The highest current value is observed at the applied potential of 0.6 V from the passive region.

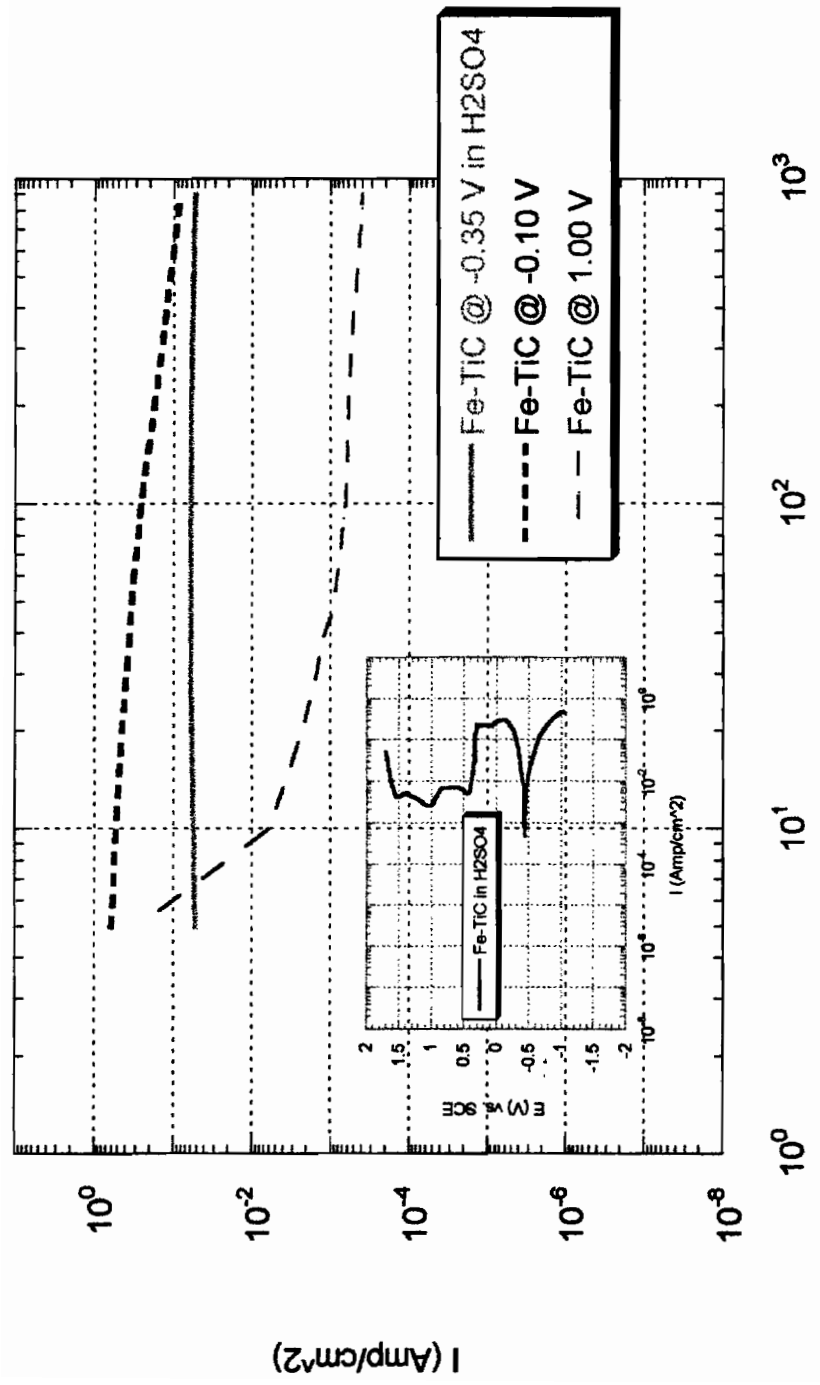

Figure 4-4-1. Current-Time Curves for Fe-TiC in H2SO4
The anodic polarization curve is shown as a small figure.

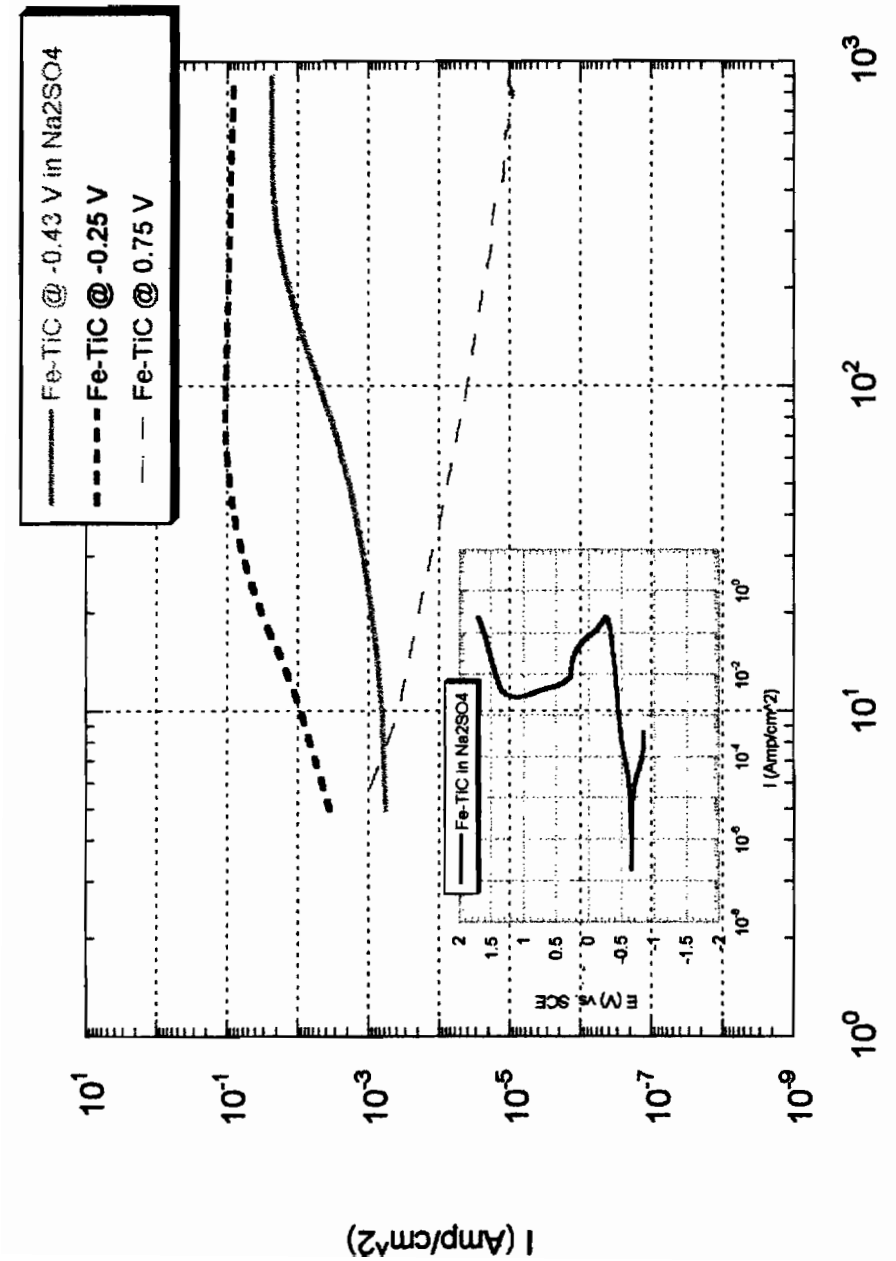

Figure 4-4-2. Current-Time Curves for Fe-TiC in Na2SO4
The anodic polarization curve is shown as a small figure.

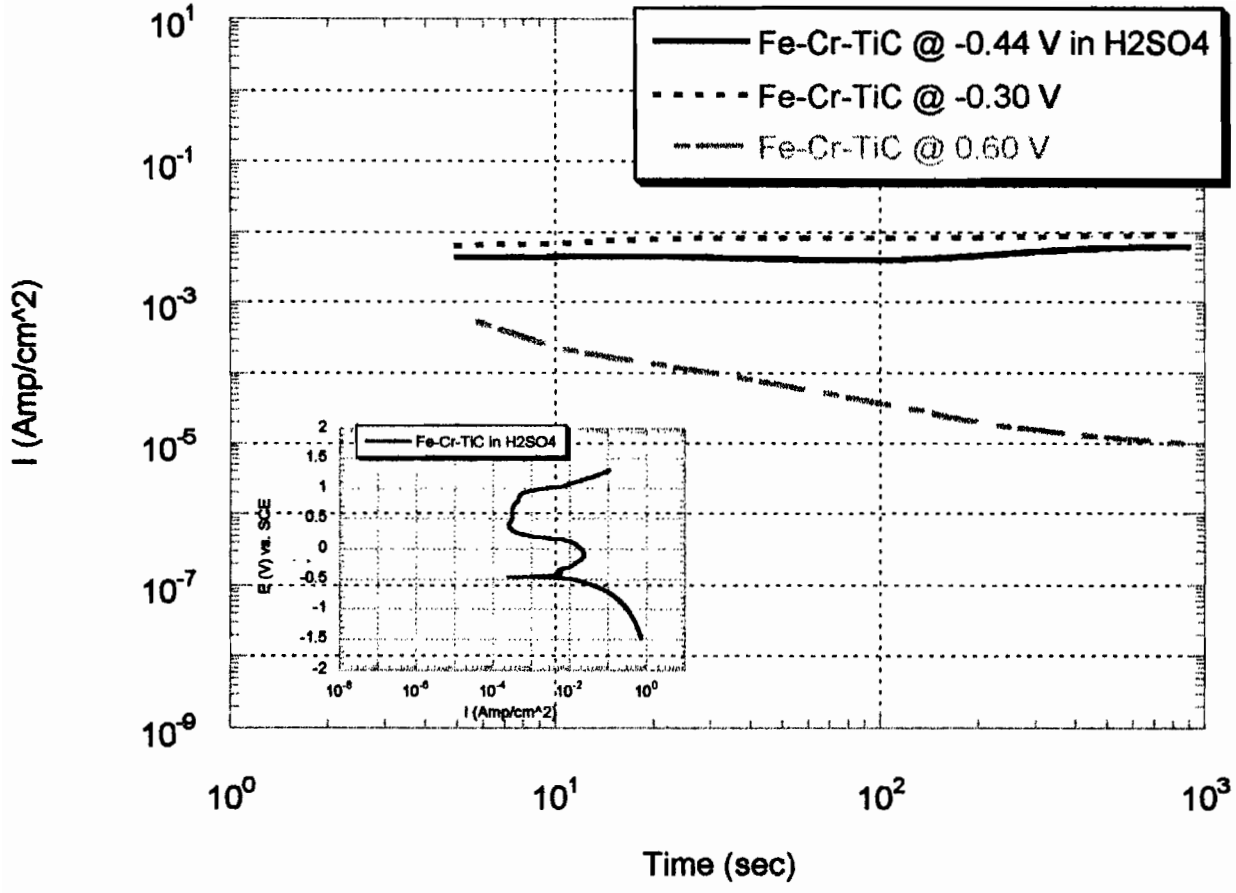

Figure 4-4-3. Current-Time Curves for Fe-Cr-TiC in H2SO4. The anodic polarization curve is shown as a small figure.

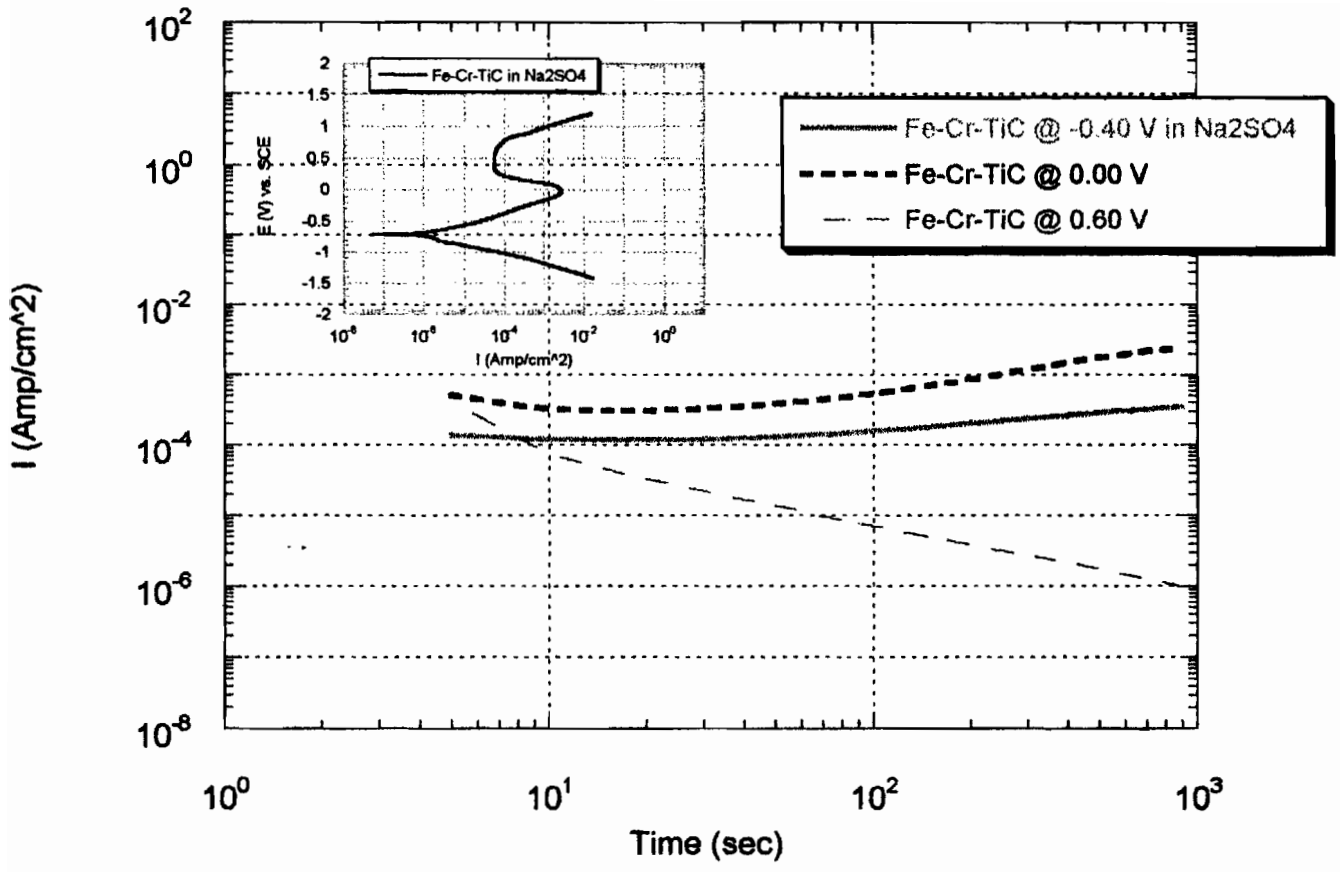

Figure 4-4-4. Current-Time Curves for Fe-Cr-TiC in Na2SO4
The anodic polarization curve is shown as a small figure.

Figure 4-4-5 shows the results of the potentiostatic experiment for Fe-Cr-Mn-TiC in the sulfuric acid solution. The highest current is observed at the E_{pp} applied (-0.46V). The second highest current is observed at the end of passive state (0.87V). The lowest current value is observed at the beginning of the passive state (0.45V).

Figure 4-4-6 shows current-time curves for Fe-Cr-Mn-TiC in the sodium sulfate solution. After 15 minutes, the highest current value is observed at E_{pp} (0.1V). After 15 minutes, the second highest current value is observed at the end of plateau (0.24V). The lowest current is observed at the passive state (0.64V).

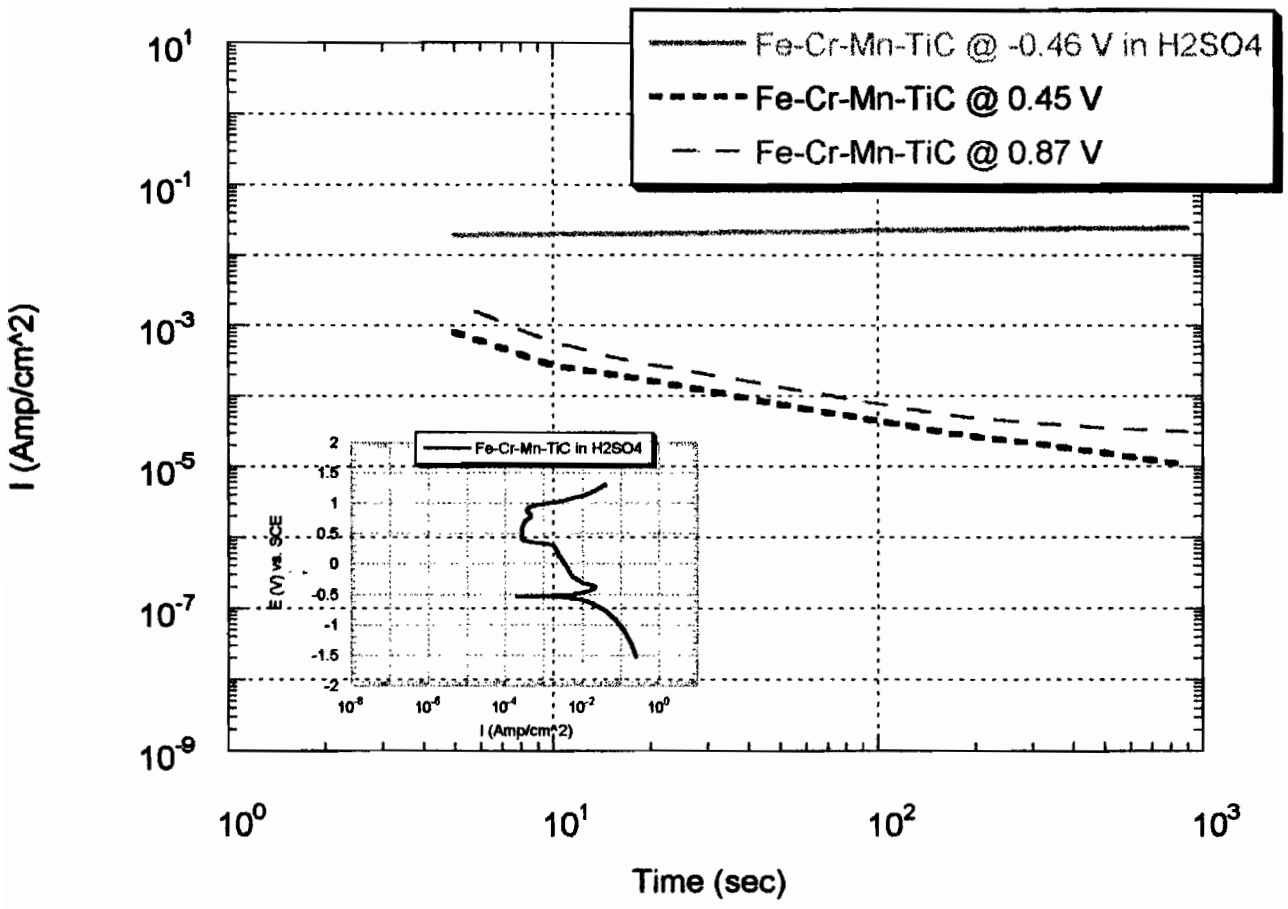

Figure 4-4-5. Current-Time Curves for Fe-Cr-Mn-TiC in H2SO4. The anodic polarization curve is shown as a small figure.

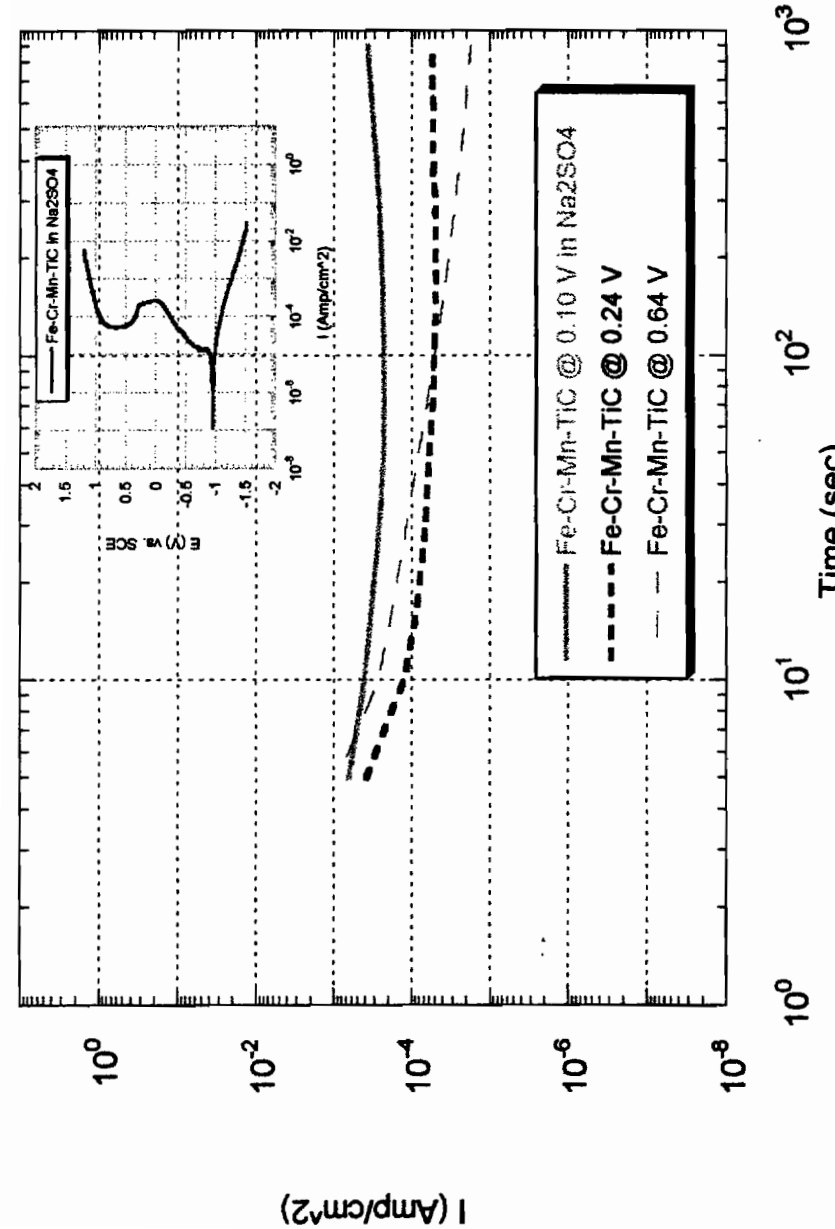

Figure 4-4-6. Current-Time Curves for Fe-Cr-Mn-TiC in Na2SO4
The anodic polarization curve is shown as a small figure.

4.5 Effect of pH on Free Corrosion Potential

Figure 4-5-1 shows the results of the open circuit potential experiments. Addition of chromium decreases the value of the open circuit potential in both the sulfuric acid solution and the sodium sulfate solution. Addition of manganese further decreases the values of open circuit potential in the both solutions.

Figure 4-5-2 and Figure 4-5-3 show the polarization curves for the investigated composites in the sulfuric acid solution and the sodium sulfate solution, respectively. The values of open circuit potentials determined in the immersion experiments are indicated in these Figures. From Figure 4-5-2 and Figure 4-5-3, the addition of chromium decreases corrosion rate in both solutions. The addition of manganese lowers corrosion rate even more.

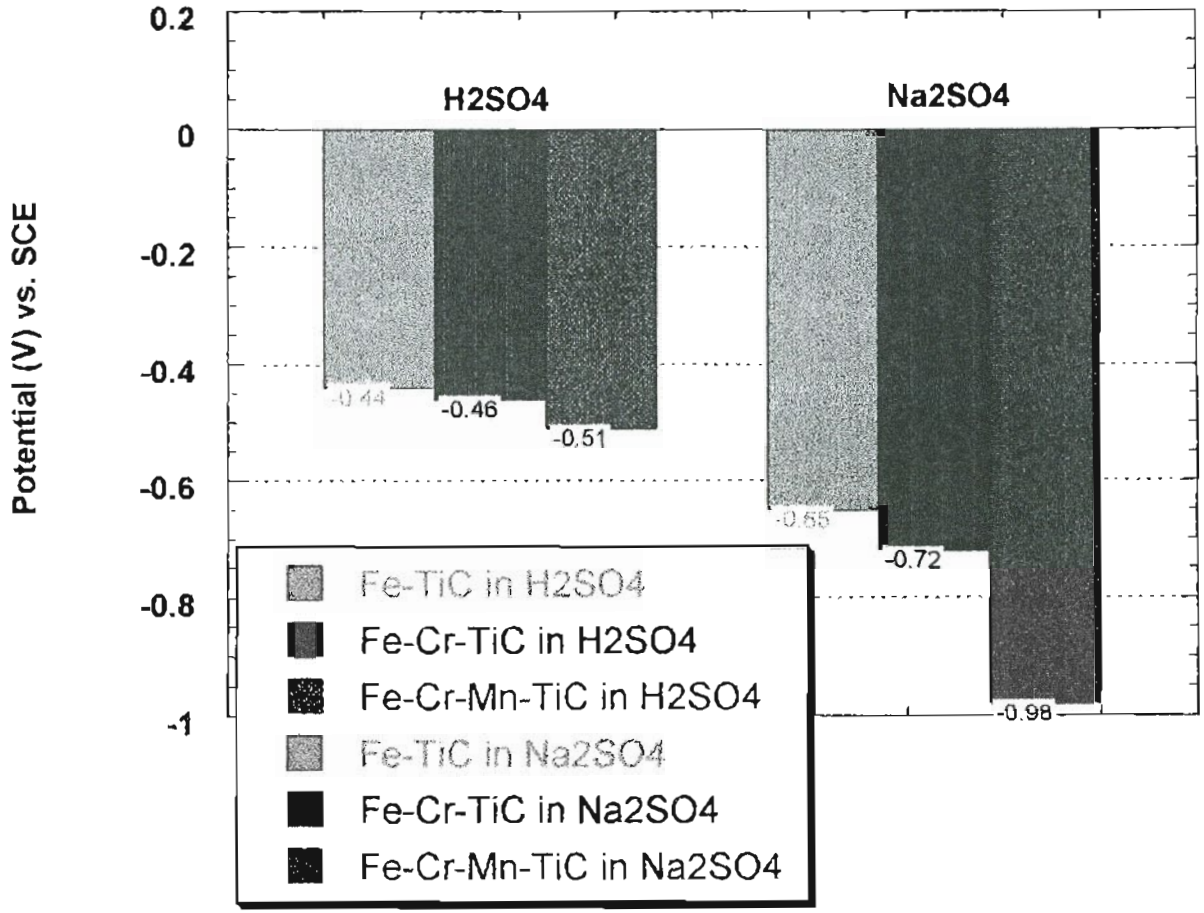

Figure 4-5-1. Open Circuit Potential Values

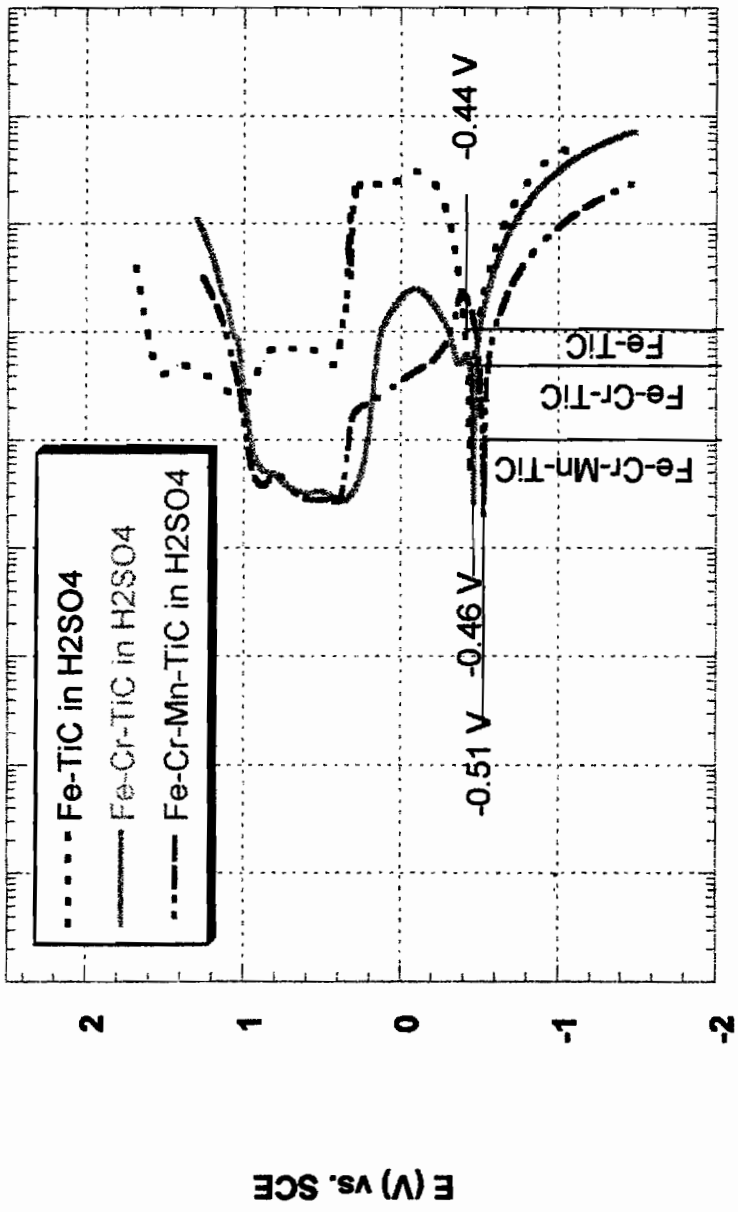

Figure 4-5-2. Effect of Chemical Composition of Composites on Open Circuit Potential in H2SO4

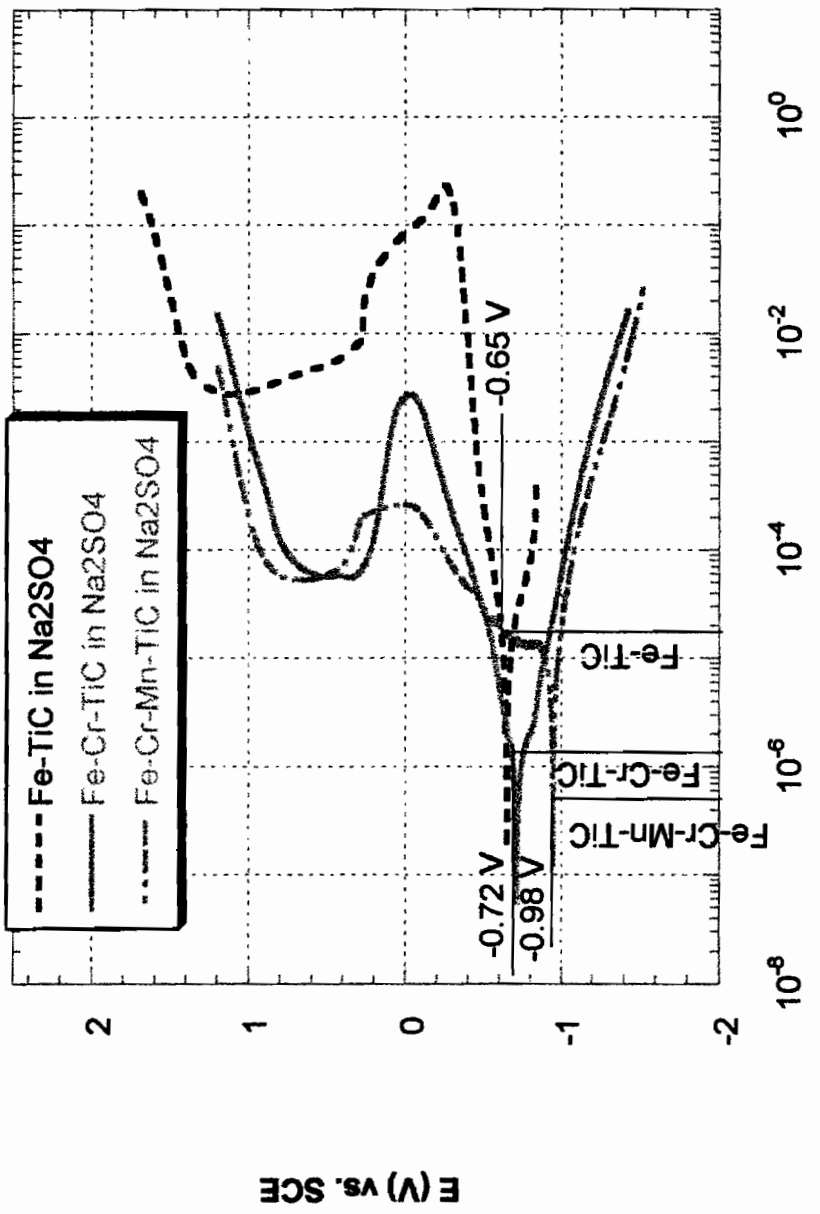

Figure 4-5-3. Effect of Chemical Composition of Composites on Open Circuit Potential in Na2SO4

Chapter 5

Conclusions

1. Based on the electrochemical experiments, Fe-TiC, Fe-Cr-TiC and Fe-Cr-Mn-TiC show passive behavior in 1N sulfuric acid solution and 1N sodium sulfate solution.
2. The addition of chromium improved the corrosion properties in both solutions in comparison to Fe-TiC.
3. The addition of manganese affected the behavior in active region in comparison to Fe-Cr-TiC.
4. Fe-Cr-TiC and Fe-Cr-Mn-TiC showed lower current densities at any applied potential value in 1N sodium sulfate than that of the sulfuric acid solution.
5. The passive films formed in sodium sulfate are more protective than those formed in sulfuric acid.

Chapter 6

Future Work

For the future work, I propose the following:

1. Perform wear experiments in order to determine the effect of wear behavior of the composites.
2. Perform Pin-on-Disc corrosion-wear experiments in order to determine the corrosion-wear performance of the composites.
3. Correlate the surface structure with the corrosion and the wear parameters by performing optical and scanning electron microscopy investigation of the composites before and after the experiments.
4. Based on the experimental results, determine the synergistic effect of corrosion and wear.

References

1. Taya, M. and R. J. Arsenault, *Metal Matrix Composites: Thermomechanical Behavior*. 1989: Pergamon.

2. Cahn, R.W., D. Bloor, R. J. Brook, M. C. Flemings and S. Mahajan. *The Encyclopedia of Advanced materials*. **2**, 1994: Cambridge University Press.

3. Pierson, H. O., *Handbook of Refractory Carbides and Nitrides*, 1996: Noyes Publications.

4. Doğan, Ö., D. E. Alman and J. A. Hawk. Wear resistant, powder processed in-situ Iron-matrix TiC composites. in *Advances in Powder Metallurgy and Particulate Materials*. ed. by T. M. Cadle and K. S. Narasimhan. pp. 83-98. 1996: Metal Powder Industries Federation.

5. Carim, A. H., D. S. Schwartz and R. S. Silberglitt., *Joining and Adhesion of Advanced Inorganic Materials*, 1993: Materials Research Society.

6. Hernandez-Guerrero, A., Z. Huque and A.M. Kanury. *An Experimental Investigation of Combustive Synthesis of Titanium Carbide*. Combustion Society and Technology. **81**. pp. 115-128. 1992.

7. Jones, D. A., *Principles and Prevention of Corrosion*. 1996: Prentice Hall, Inc.

8. Lunarska, E. and J. Michalski, Corrosion resistance of composite TiN-TiC layers deposited on tool steels by different techniques. *Journal of Materials Science*. **30**. pp. 4125-4132. 1995.

9. Walton, C. F., *Gray and Ductile Iron Casting Handbook; Including data on Gray, Ductile, White and High Alloy Irons*, 1971: Gray and Ductile Iron Founders' Society Inc.

10. Ochiai, S., *Mechanical Properties of Metallic Composites*. 1994: Marcel Dekker Inc.

11. Uhlig, H. H. and R. W. Revie, *Corrosion and Corrosion Control.* 1985: John Wiley & Sons.

12. Oblonsky L. J., M. P. Ryan and H. S. Isaacs, In situ determination of the composition of surface films formed on Fe-Cr alloys. *Journal of The Electrochemical Society.* **145** (6) pp. 1992-1932. 1998.

13. Fontana, M. G., *Corrosion Engineering.* 1986: McGraw-Hill Book Co.

14. Wranglen, G. *An Introduction to Corrosion and Protection of Metals.* 1985: Chapman and Hall.

15. Madsen, B. W., Corrosive Wear. *ASM Handbook: Friction, lubrication, and wear technology.* **18**. pp. 271-279. 1992: ASM International.

16. Friedersdorf, F. J. and G. R. Holcomb, Pin-On-Disc Corrosion-Wear Test. *Journal of Materials Testing and Evaluation.* **26**. (4) pp.352-357. 1998.

17. Pourbaix, M., *Atlas of Electrochemical Equilibria in Aqueous Solutions.* 1966: Pergamon Press.

Biography

The author was born in October 6th, 1967 in Tokyo, Japan. She graduated from Fujimigaoka high school in Japan in 1986. She graduated from Portland Community College with A.A.S. in Mechanical Engineering Technology in 1994. Then, she continued her education at Oregon Institute of Technology. She received her B.S. degree in Mechanical Engineering Technology in 1996 with Cum Laude. The same year, she joined the Department of Materials Science and Engineering at the Oregon Graduate Institute of Science and Technology to work her M.S. degree.